Chapter-4

Cellulose-based Luffa Cylindrica (Mat, Flakes, and Powder) Reinforced Polydimethylsiloxane Composites for Oil and Organic Solvent Absorption

4.1 Introduction

In recent decades, oil spills and organic solvent-based seepage have become one of the greatest hazards to our living ecosystems and are causing health issues (H. Singh et al. 2020; Wolok et al. 2020). Increasing production, transportation, and storage amounts of crude oil raise the potential of oil spills in marine and freshwater settings. Numerous high-profile spills have occurred in recent decades, inflicting not just the loss of energy resources but also considerable damage to the environment and ecosystems (Abdelwahab 2014; Guo et al. 2019). When oil spills occur, harmful substances such as polycyclic aromatic hydrocarbons are released into the environment. These hydrocarbons are toxic to humans as well as aquatic life, and it may take decades to eradicate them (Adebajo et al. 2003; Solomon and Janssen 2010).

The oil spillage can produce an oil-water emulsion or layer of thin films, both limiting the entry of sunlight and ultimately contributing to the death of living creatures that reside inside the water body (Abdelwahab 2014; Cirer-Costa 2015; M. Yu et al. 2018). It is becoming imperative to develop efficient, cost-effective sorbent material to remove oil spillage to mitigate the harmful effects of oil spills on the environment. Several diverse methods are available to clean up oil spills, including centrifugation, skimming, filtering, chemical treatments, in situ combustion, bioremediation, adsorption and absorption. Among all, adsorption and absorption are the most popular techniques since they require less energy and could recover oil spillage (Wolok et al. 2020). Nevertheless, the choice of absorbent materials is essential. There are several absorbent materials, particularly sponges, films, membranes, meshes, aerogels and composites made up of natural and synthetic materials have gained much attention due to their efficacy for efficiently removing oily pollutants from water/environment. Synthetic materials such as polypropylene, carbon nanotubes, polydimethylsiloxane (PDMS) and graphene-based sponges that are hydrophobic show high absorption capacity (Ge et al. 2021; L. Liu et al. 2020; Ong et al. 2018; Vagos et al. 2020; Zheng et al. 2022). However, they noticeably suffer from

technical complications related to their complex synthesis or modification procedures and scaling issues that must be addressed (Choi et al. 2011; W. Zhang et al. 2021). Researchers are extensively interested in absorbents derived from natural materials since they play a key role in separating oil from water surfaces. According to the literature, various natural materials such as cotton fibers, coconut husk, treated bark and kapok fibers have been reported to clean up oil spills from water. However, their low absorption capacity, poor oil/water selectivity, sinking after sorption and limited reusability impeded their practical applicability (Ali et al. 2011; Futalan et al. 2022; Lv et al., n.d.; Sayed and Zayed 2006; Senanurakwarkul et al. 2013; Z. Wang et al. 2017). Lightweight, cost-effective and eco-friendliness are three main requirements for manufacturing highly effective absorbent materials. Therefore, there is an immediate requirement for the modification of natural materials to facilitate the fabrication of cutting-edge, technologically sophisticated absorbent materials as well as effective approaches to remove organic solvents and oils from water (Ge et al. 2021).

The present work is to investigate the various forms of natural luffa cylindrica mat (LC), which is modified into different forms, i.e., luffa flakes and luffa powder. Further, LC forms have been impregnated with PDMS using the hand lay-up technique. The four designed scaffolds are P-L mat, P-L flakes, P-L powder and PDMS (P). The PDMS is a silicon elastomer-based polymeric material used in numerous science, engineering, environmental, and general applications due to its favorable properties, including flexibility, transparency, non-toxicity, chemical inertness, biocompatibility, water resistance, excellent elasticity, hydrophobicity, oxygen permeability, thermal stability and excellent elasticity (Akther et al. 2020; Miranda et al. 2021; Zhai et al. 2021). As a result, PDMS has recently gained recognition as a promising tool for oil removal for environmental restoration. Several researchers have reported on the utilization of PDMS as a promising absorbent material for the removal of oil and organic pollutants from water. In particular, Guo et al. have designed PDMS sponges for oil and organic

solvent absorption (Guo et al. 2019). In another work, Bayraktaroglu et al. fabricated hydrophobic PDMS scaffolds via bulk polymerizing tetraethyl orthosilicate (TEOS) to cleanup water from oil and solvents (Bayraktaroglu, Kizil, and Bulbul Sonmez 2021). Khan et al. fabricated nanosponges using PDMS-luffa-titanium dioxide materials to harvest oils from diatom cultures (M. J. Khan et al. 2019). Due to the aforementioned characteristics, PDMS was chosen as the material of choice for regulating the floating capabilities, oxygen permeability and loss of gaseous exchange of scaffolds that takes place between the air and the water body.

Luffa cylindrica (LC) is a sponge material with a fibrous network. It is a hydrophilic material with 60% cellulose, 30% hemicellulose, and 10% lignin. LC is a climbing plant that grows yearly and bears fruit with fibrous vascular systems. They have been grown for a very long time in the tropical regions of Asia and Africa. LC has demonstrated substantial advantages as a material for reinforcement, as a bath sponge, dishwasher scrub, shock absorber, packaging material, and as an absorption material in water treatment (Gundu et al. 2022). Luffa possesses microcapillary activity, one of the primary properties allowing it to absorb fluids. Micropores or channels, surface tension and adhesion forces between a fluid and a material attract fluids to move inside due to capillary action. The material comprises a network of small capillaries and channels that can absorb oil due to its fibrous structure. Several investigations have demonstrated that the components derived from luffa plants can potentially be utilized to remedy oil spills. In a study, it was revealed that luffa fibers were selective for oils and resisted water absorption. According to studies, absorption was dependent on soaking time and absorbent concentration. The absorption capacity of luffa fibers was found to decrease with increasing temperature, and maximal absorption was observed at 40 °C (Abdelwahab 2014; Anastopoulos and Pashalidis 2020). Studies have revealed that large fiber capillaries improve oil absorption and retention (Xu et al. 2021). The mechanism of oil sorption by its hollow fiber may be adjusted by surface sorption and capillary action (Abdelwahab 2014). In a study by

Wang et. al., a porous natural luffa sponge with a fibrous network structure was exploited for oil absorption. Due to its porosity, the luffa sponge may be used as a filter and absorbent in the dye removal process. Super-hydrophobic luffa sponges with excellent absorption capacity were developed through surface modification with polyhedral oligomeric silsesquioxane (POSS) (Z. Wang et al. 2017). Thus, the components i.e., luffa and PDMS are well known to exhibit the properties to absorb oil/petroleum products.

This novel work aims to demonstrate various forms of luffa-PDMS-based scaffolds by a simple hand lay-up procedure to understand which form of luffa-PDMS scaffolds possesses greater efficacy in separating oil from water. To the best of our knowledge, we present for the first time luffa in three different forms i.e., mat, flakes, and powder embedded with PDMS using a simple fabrication technique. The PDMS is a hydrophobic material expected to avoid sinking the scaffolds inside the water against gravity. In addition, the PDMS also has the property of absorbing traces of harmful organic solvents enabling the luffa-PDMS to be a highly efficient material for oil absorption. Therefore, PDMS and luffa-based scaffolds are expected to eradicate major (organic and inorganic) pollutants from the environment. It is envisaged that the non-porous PDMS materials will absorb organic solvents enabling the scaffold to float over the water body. In addition, it is anticipated that the luffa cylindrica will enhance oil absorption. Out of the four different types of scaffolds prepared, the P-L flakes are found to give the best efficiency for oil absorption. This is attributed to the fact that they possess a high surface area-to-volume ratio and high interconnectivity inside the microporous structure. Several characterizations, including oil absorption, oil-water separation, surface wettability, organic solvent absorption, surface roughness and thermogravimetric analysis, have been performed to determine the optimal and most effective scaffold combination.

4.2 Materials and method

4.2.1 Materials

LC dried fruits were attained from a local supermarket in Varanasi, Uttar Pradesh, India. The PDMS silicone elastomer and curing agent (Sylgard 184) were acquired from Dow Corning Corporation (USA). Sodium hydroxide (NaOH) was purchased from Qualigens, Mumbai. Dulbecco's modified Eagle Medium (DMEM), fetal bovine serum (FBS), lysozyme (10^4 U/mL), trypsin- EDTA, antibiotic penicillin, Phosphate buffered saline (PBS), paraformaldehyde, 3-[4, 5- dimethyl- thiazol-2-y1])-2, 5-diphenyltetrazolium bromide (MTT) assay kit were procured from Himedia. Toluene, cyclohexane and dimethyl sulfoxide (DMSO) and calcium carbonate ($CaCO_3$) were obtained from the Sisco Research Laboratory. Absolute ethanol (99.9% high analytical grade) and pure distilled water were utilized to treat LC fibers. Motor oil was purchased from the local market in Varanasi, Uttar Pradesh, India. Diethyl ether and n-hexane were purchased from Loba Chemie. MG-63 [Human osteoblast] cell line was procured from National Center for Cell Science (NCCS), Pune, India.

4.2.2 Methods

4.2.2.1 Modification of LC fibers through chemical treatment

Initially, the outer layer of dried luffa mat (L-mat) was cut into small portions and washed thoroughly with distilled water to eliminate gummy and residual particles. The fibers were dried in an oven at 60°C for 24 h. In a 2M NaOH solution, the fibers were heated to 120°C for 2 h. To obtain a neutral pH, chemically modified fibers were rinsed with distilled water and dried at 60°C in a hot air oven for 48 h. The luffa flakes (L-flakes) were obtained by coarsely grinding them in the grinder. Furthermore, the modified luffa flakes were grounded into a fine powder (L-powder) in a rotary machine for 2 h using pure (99%) absolute ethanol.

4.2.2.2 Fabrication of Luffa-PDMS scaffolds

The luffa-PDMS-based hybrid composite scaffolds were fabricated by layering the luffa fiber mat in a mold and impregnating it with PDMS using the hand lay-up technique. Four scaffolds of various combinations were prepared by adding 1 g of modified LC fiber mat in 4 g of PDMS to prepare the P-L mat scaffold. 1 g of luffa flakes was added to 4 g of PDMS to prepare the P-L flakes scaffold, 1 g of luffa powder was added to 4 g of PDMS to prepare P-L powder scaffold and 4g of PDMS alone to prepare a control scaffold. Formulations of different composites are tabulated in Table 4.1. The combinations were categorized accordingly as P-L mat (LC mat/PDMS), P-L flakes (LC flakes/PDMS), P-L powder (LC powder/ PDMS), and control (PDMS (P)). Initially, the weighing of the various forms of LC material, i.e., mat, flakes, and powder, was performed and then placed into the molds. 4 g of PDMS (10:1) was prepared by vigorously mixing both the elastomer and the curing agent for 15 min, which was later degassed until all air bubbles were eliminated.

Further, PDMS was poured onto the layered luffa mold in both cylindrical and rectangular shapes with a dimension of 130 mm x 10 mm x 3 mm, and they were cured in a hot air oven at 60°C for 4 h. Similarly, the other combinations of scaffolds were prepared. After curing, the fabricated luffa/PDMS-based scaffolds were obtained (Figure 4.1). During characterization, the scaffolds were sliced into cross-sections (i.e., circular discs) to expose the LC portion more from both ends.

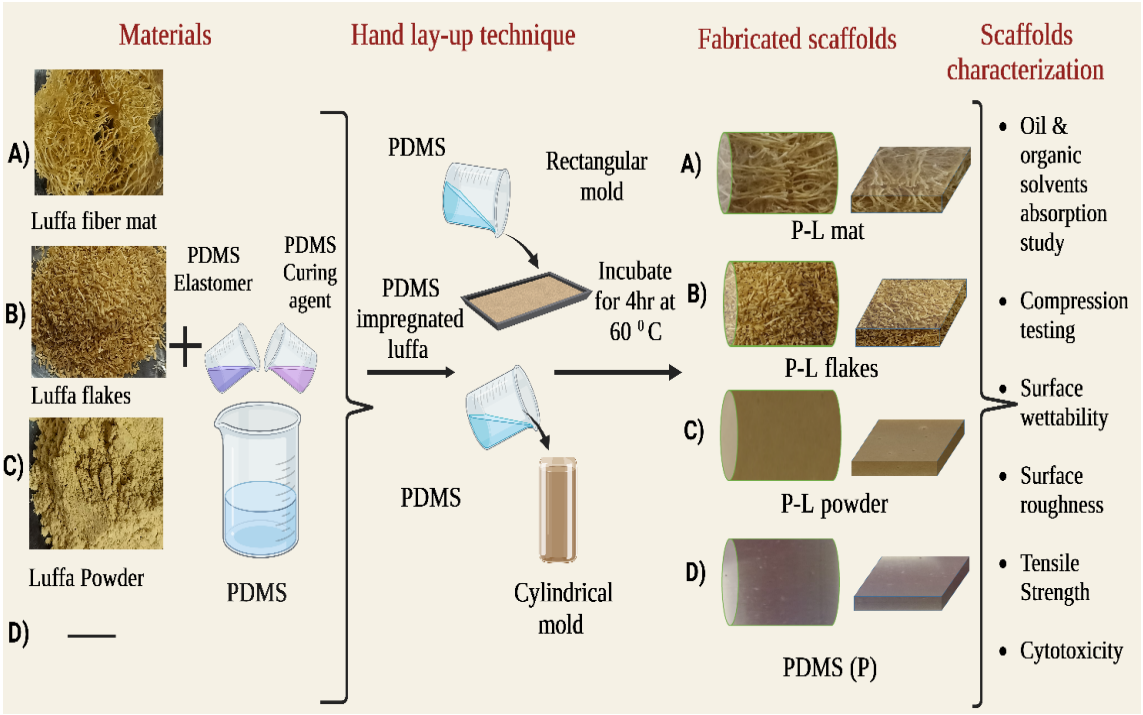

Figure 4.1: Schematic representation of scaffold fabrication of (A) P-L mat, (B) P-L flakes, (C) P-L powder, and (D) PDMS (P) scaffolds using a hand lay-up technique.

Table 4.1: Represents the composition of various forms of luffa-PDMS- based scaffolds, i.e., types of scaffolds and their composition.

Types of Scaffolds and their composition				
S.No.	**Scaffold Name**	**Luffa Cylindrica (LC)**	**PDMS (P)**	**Ratio (LC: PDMS)**
1.	P-L mat	LC mat 1g (25% w/w)	4g (75% w/w)	1:4
2.	P-L flakes	LC flakes 1g (25% w/w)	4g (75% w/w)	1:4
3.	P-L powder	LC Powder 1g (25%w/w)	4g (75% w/w)	1:4
4.	PDMS (P)	------	4g (100% w/w)	0:4

4.2.3 Characterization of fabricated scaffolds

4.2.3.1 Morphological and surface roughness analysis using scanning electron microscopy (SEM)

To evaluate the morphology and the surface roughness of fabricated scaffolds, field emission SEM (Nova NanoSEM 450) and conventional SEM (A Zeiss EVO 18 SEM, Oberkochen, Germany) were utilized. The small portion of scaffolds was punched and coated with gold, and a voltage of 20 kV was used to capture images of the scaffolds. ImageJ software (NIH, USA) was used to measure the surface roughness. The surface roughness was calculated using the following procedure 1) firstly, ImageJ software was opened, 2) an image was dragged and a scale bar was set there, 3) the analysis option was clicked and then plot profile was selected, 4) the image was converted to 32-bit, 5) through plugins SurfCharJ 1q a desired image was obtained.

4.2.3.2 Surface roughness using atomic force microscopy (AFM)

Atomic force microscopy (AFM) is a widely accepted technique for measuring the surface roughness of materials with high precision and accuracy. The images were captured in the air atmosphere on (NT-MDT), NTEGRA prima instrument (Russia). The surface roughness of fabricated scaffolds was analyzed under semi-contact mode with a scan speed of 0.5 Hz using Nova_ Px software. The acquired data were processed to produce a topographic image of the surface, from which the roughness was calculated. The root means square roughness (Rq) is commonly used to quantify the surface roughness and to detect changes in the height of roughness due to the availability of the pores or voids.

4.2.3.3 Effective porosity of the scaffolds

To determine the effective porosity of scaffolds, samples of a 10 mm diameter and 3 mm height, i.e., P-L mat, P-L flakes, P-L powder, and PDMS (P) were weighed (W_d i.e., dry weights), and later the samples were soaked in 99.9% absolute ethanol overnight to allow ethanol to permeate

into the scaffolds, a repeated cycle of vacuuming and degassing air in a desiccator under a vacuum was performed. After being saturated with ethanol, the samples were reweighed to determine the weight gain, denoted as 'W_w' (i.e., wet weights). The effective porosity (P_E) of the scaffold was calculated as shown below:

$$P_E = \left(\frac{W_w - W_d}{\rho_{ethanol} V}\right)$$

Where W_d and W_w are the weights of the scaffolds before and after immersion in ethanol. ρ is the density of ethanol (i.e., 0.789 g/cm^3), and V is the apparent volume based on scaffold dimension.

4.2.3.4 Thermogravimetric analysis (TGA)

The thermal stability of the scaffolds was measured by a TGA-50 thermogravimetric analyzer (Shimadzu (Asia Pacific) Pvt. Ltd). The sample of 5 mg was placed into the instrument and heated at a rate of 10°C /min at temperatures ranging from 20 to 500°C. TGA provides weight loss with respect to time, temperature and environment to assess the material's thermal stability.

4.2.3.5 Surface wettability measurement

The surface wettability was measured to analyze the hydrophobic and hydrophilicity of the scaffolds. 10 µL of distilled water has been utilized as a reference to define the contact angle of the scaffolds. On every scaffold, 10 µL of a water droplet was pipetted on the surface of the scaffold using a micropipette and the images were captured at a certain time i.e., 0, 30, 60, and 90 minutes using a digital camera (Canon 1500D). The contact angle has been measured with a drop analysis (LB-ADSA) plugin from ImageJ software. The mean and standard deviation were calculated by considering three sets of all the scaffolds to determine the contact angle.

4.2.3.6 Absorption of oil, PBS, and organic solvents by the prepared scaffolds

The ability of the composite scaffolds to absorb oil, PBS, and organic solvents was evaluated by immersing scaffolds of 3 mm thickness and 10 mm diameter for 72 h at 37℃ in motor oil, PBS solution (pH of 7.4) and various organic solvents, including diethyl ether, cyclohexane, n-hexane and toluene. For performing experiments, 15 mL volume was used for organic solvents, oil and PBS to immerse the scaffolds. To ensure their accuracy, samples in triplicate of different combinations were studied. Using a weighing balance, the weights of scaffolds immersed in PBS solution, motor oil, and organic solvents were obtained at predefined intervals by removing excess fluids with tissue paper. The absorption percentage was computed using a formula.

$$\text{Absorption (\%)} = \left(\frac{W_w - W_d}{W_d}\right) \times 100$$

Where W_d and W_w represent before and after immersion of various combinations of scaffolds, respectively, into oil, PBS, and organic solvents.

4.2.3.7 Oil-water sorption study

For the oil-water sorption study of the scaffolds, five separate glass beakers, each containing 15 mL of water, were used. One milliliter of motor oil was then carefully dropped into each beaker containing water, then variable types of scaffolds were gently placed into the respective beakers allowing them to absorb oil/water. After a predetermined time, i.e., 24 h, the scaffolds were blotted with tissue paper to remove excess oil and then weighed. The absorption capacity of the scaffolds was quantified using the final weight after 24 h and the initial dry weight of the scaffolds. To identify absorbed liquids, the scaffold was removed from the surface of the oil and water mixture, and the wet absorbent material was weighed after being drained for 1 min in a 70 µm strainer. To determine the exact value of water and oil sorption, scaffolds were

incubated in a hot air oven at 60℃ for 1h, followed by incubation of scaffolds in a $CaCO_3$ pellet-containing chamber for 48 h to remove the water content of scaffolds.

4.2.3.8 Reusability of fabricated scaffolds

A recyclability assessment was conducted for the developed scaffolds by immersing them in a Petri dish containing 3 mL of water and 50 µL of motor oil. This method was employed to determine the scaffold's effectiveness in terms of its ability to be recycled. The samples were subjected to hot water for washing, dried at 60℃ for 30 min and then re-submerged in the oil-water mixture for the next cycle after each test. The subsequent evaluation was performed for all the scaffolds.

4.2.3.9 Mechanical characterization of scaffolds

Compression and tensile properties of various combination scaffolds were tested using Instron 5982 Universal Testing Machine (UTM) by maintaining ASTM (American Society for Testing and Material International) guidelines for testing and evaluating materials. A total of three sets of scaffolds (n = 3) were used for the assessment having dimensions of 20 ± 1.0 mm height x 10 ± 1.0 mm diameter for the compression test and 100 mm x 10 mm x 3 mm for a tensile test with 2 mm/s of speed using 100 kN load cell. Bluehill-3 software was used to assess the load-displacement findings, and using OriginPro 2020 (OriginLab, Learning edition), Young's modulus was computed according to the data obtained.

4.2.3.10 Cytotoxicity

The cytotoxicity and cell proliferation on fabricated scaffolds were evaluated using MG-63 [Human osteoblast] cells through an MTT reduction assay. To improve the interaction between the cells and the material, the internal surface of the scaffold has been modified by subjecting it to plasma treatment for one minute. Further, using standard procedure, the cells (1×10^4 cells per scaffold) were seeded on a 96-well plate and placed in a CO_2 incubator for 4 days at 37℃

with 5% CO_2. Each experiment was carried out in triplicates to test the prepared scaffold's cytotoxicity and biocompatibility. For the process of MTT assay, the growth medium was discarded, and the scaffolds were carefully shifted to a new well to prevent erroneous data reading due to the adhesion of cells to the well during incubation, followed by the addition of 10% MTT in the culture medium. The scaffolds immersed in a medium containing MTT solution were further incubated for 4 h to permeate MTT inside the live cells and formation of formazan crystal. The products of the formazan reaction were dissolved in dimethyl sulfoxide for 30 min after transferring the scaffold to a fresh well. The dissolved formazan solution was transferred to a new flat bottom 96-well plate. The optical absorbance was measured at the wavelength of 570 nm on an immunosorbent assay (ELISA) reader (Synergy H1 hybrid, Biotek, USA).

4.2.3.11 Biodegradation of scaffolds

The degradation of the scaffolds was examined by immersing specimens in a PBS buffer containing lysozyme solution (10^4 U/mL) at 40°C for monitoring the weight loss of scaffolds over 20 days. At a predetermined period, the scaffolds were taken out of the medium, washed with distilled water, and freeze-dried to obtain the weights of the scaffolds. The experiment was performed in triplicates of samples, and the obtained values were considered to calculate the degree of deterioration. The weight loss percentage was measured from the formula given below:

$$\text{Weight loss (\%)} = \left(\frac{W_i - W_f}{W_i}\right) \times 100$$

Where W_i and W_f denote the initial and final weights of the scaffolds before and after deterioration, respectively.

4.2.3 Statistical analysis

All the studies were carried out in triplicate to assure repeatability and statistical analysis, and the outcomes were expressed as the mean and standard deviation (SD). All the experimental data were statistically analyzed using one-way analysis of variance (ANOVA) and Tukey's Post hoc multiple comparison tests. The obtained data was analyzed using OriginPro 2020 (OriginLab, Learning edition) to plot all the graphs.

4.3 Results

4.3.1 Characterization of the scaffolds

4.3.1.1 Morphological characteristics and surface roughness analysis of the fabricated scaffolds

The morphological characteristics of the fabricated three-dimensional architecture were examined through scanning electron microscopic (SEM) images. Figure 4.2 represents the SEM images, their respective surface roughness, and a graphical representation of roughness intensity and frequency. Table 4.2 represents various parameters of surface roughness. The distribution of grey values at each point of the SEM image is used as an index of the surface roughness for every scaffold. The scaffolds with luffa fibers (P-L mat) exhibited high-intensity peaks with the least frequency. The highest frequency with continuous peaks was observed in P-L powder scaffolds, representing the highest roughness. Least/negligible peaks were obtained on PDMS (P) surface, probably because of an absence of luffa. A few peaks observed in the PDMS (P) graph might have resulted due to deposition of dust or foreign particles. Medium-sized luffa flakes, i.e., P-L flakes, exhibited average peaks with peaks less than P-L powder but higher than P-L mat. In 3D reconstructed images, the surface of PDMS (P) seems smoother than that of other scaffolds. As a result of the roughness comparison, the P-L mat and P-L flakes were observed to possess significantly greater crests spread over the scaffold surfaces (Figure 4.2 A & B). Since luffa mats and flakes exhibited a more fibrous structure and irregular pattern, the resulting scaffold was found to have a noticeably greater number of pores

and a significantly higher crest than P-L powder. Since P-L powder consisted of very minute particles of luffa that were organized homogenously throughout the structure, resulting in the scaffold displaying very little evidence of crest on the surface (Figure 4.2 C). The PDMS (P) scaffolds exhibited significantly no crest, most likely due to the absence of luffa, and its surface was considered smooth with respect to the other scaffolds (Figure 4.2 D).

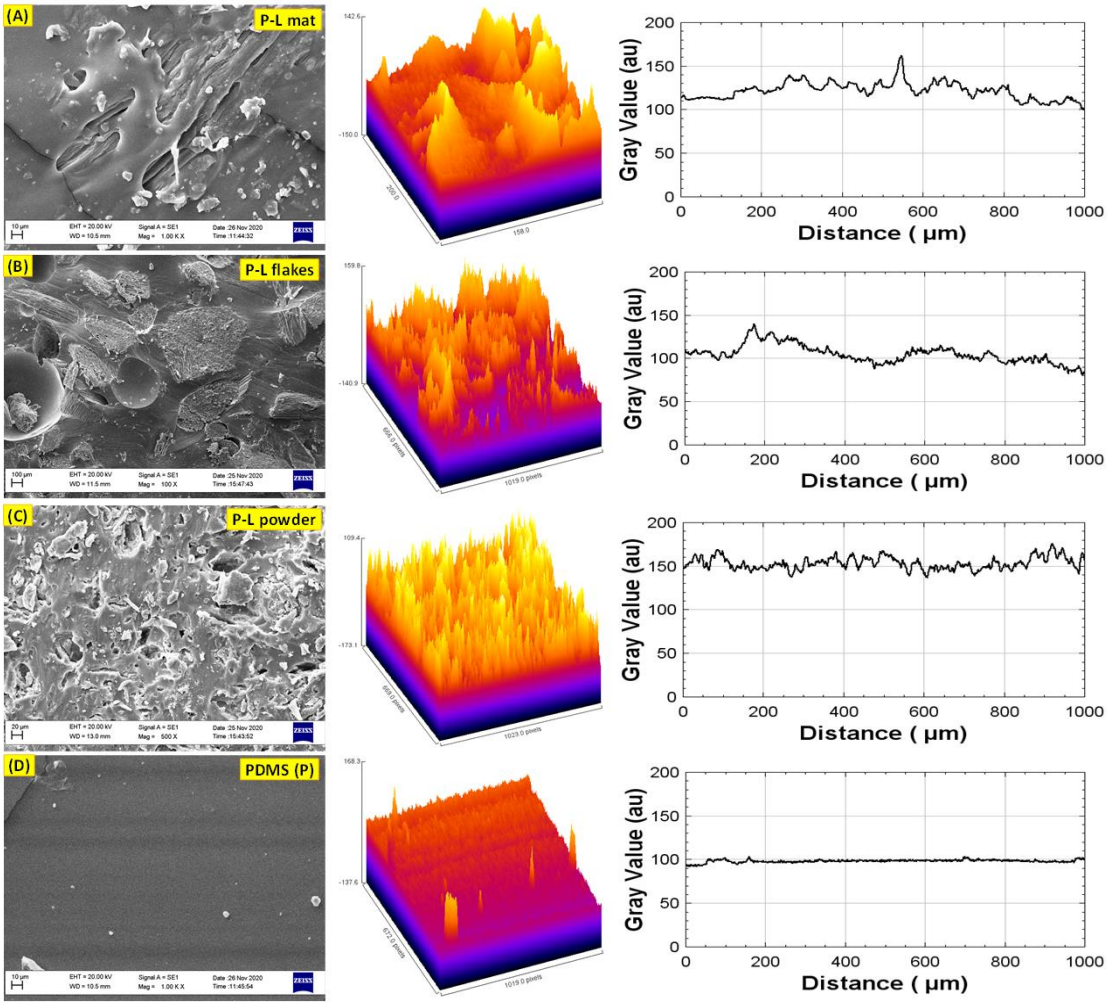

Figure 4.2: Morphological analysis through scanning electron microscopy (SEM) photomicrograph of (A) P-L mat (B) P-L flakes (C) P-L powder and (D) PDMS (P) scaffolds along with their respective surface roughness and grey value peak intensity to justify their surface roughness.

Table 4.2: Surface roughness parameters (A) P-L mat (B) P-L flakes (C) P-L powder and (D) PDMS (P) scaffolds quantified using Surf CharJ 1q plugin of ImageJ. Units= arbitrary units (au). Data were analyzed using One-way ANOVA Tukey's Post hoc Test.

S. No	Name	Root mean square deviation (Rq)	Arithmetical mean deviation (Ra)	Lowest valley (Rv)	Highest peak (Rp)	Total height of the profile (Rt)	Surface area (SA)
1.	P-L mat	36.923	28.222	-95.398	120.494	215.892	9.786
2.	P-L flakes	42.376	33.991	-99.628	123.780	223.408	13.193
3.	P-L powder	49.452	40.673	-142.64	97.242	239.884	15.686
4.	PDMS (P)	24.112	19.223	-71.149	86.436	157.586	10.434

To visualize the topography and the three-dimensional (3D) architecture of the fabricated scaffolds, we have captured digital images and performed SEM analysis that demonstrates the internal architecture of luffa embedded in PDMS (Figure 4.3). The digital images of the scaffold were captured from multiple angles to confirm the 3D architecture of the scaffold and the distribution of luffa. The SEM images of the P-L mat illustrated the luffa mat embedded within the reinforcing material (PDMS) that was observed in various magnifications. The internal architecture of luffa depicted presence of the microcapillaries and the microporous structures. It was also observed that the luffa fibers were in low abundance but were found continuously present throughout the scaffold. The luffa flakes in the P-L flakes scaffold were found randomly arranged within PDMS. P-L flakes scaffold demonstrated a high density of luffa microparticles with high surface area to volume exposed, which resulted in the highest

absorption compared to other scaffolds. Since the P-L powder is a fine powder with micron size, most of their capillaries were found compromised; resulting in densely packed within PDMS material and appearing as agglomerated materials when seen under different magnifications. The PDMS (P) alone material appeared smoother than the P-L mat and P-L flakes-based scaffolds. Moreover, high-density packing with the less porous architecture of the P-L powder significantly resulted in less oil absorption. In contrast, the PDMS alone appeared smooth and pore-free.

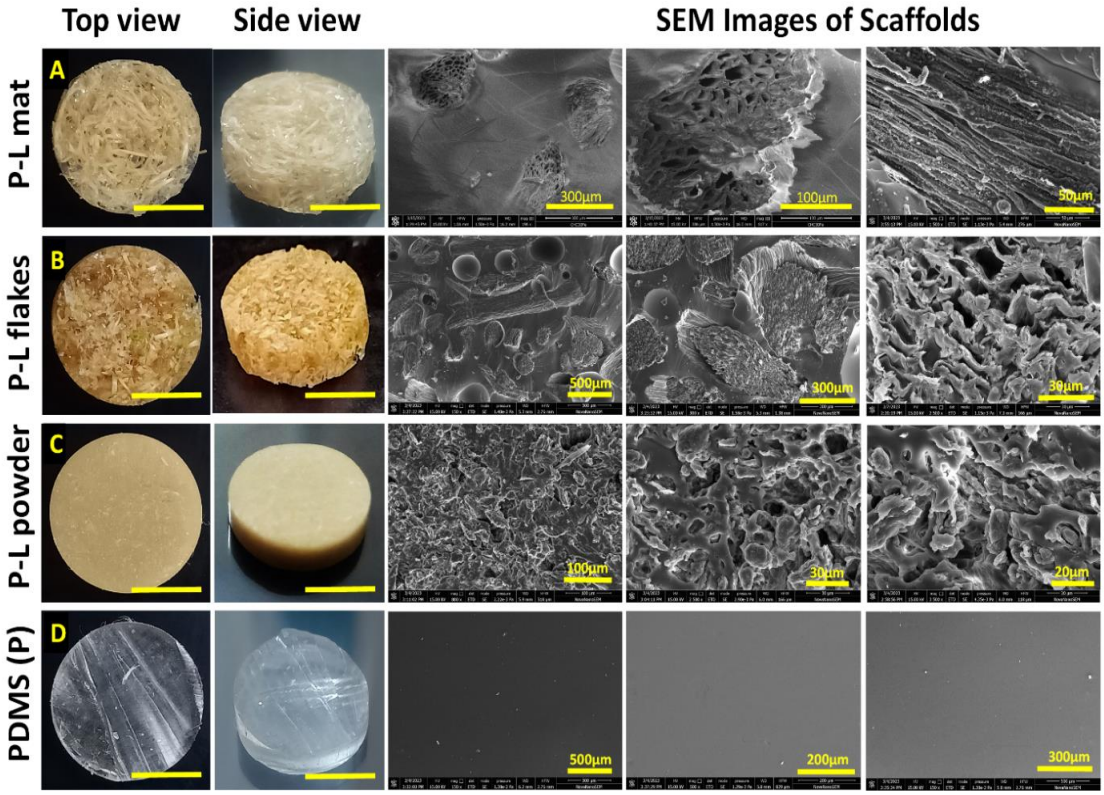

Figure 4.3: Represents the digital images of scaffolds (A) P-L mat, (B) P-L flakes, (C) P-L powder, and (D) PDMS (P) in top and side view and SEM images of the respective fabricated scaffolds with various magnification. Scale bar: 10 mm.

4.3.1.2 Surface roughness analysis (AFM)

To investigate the scaffold's surface roughness (Rq), atomic force microscopy (AFM) was used. Figure 4.4 depicts the two-dimensional (2D) and three-dimensional (3D) topographical view using non-contact mode. Since P-L mat scaffolds possessed a high mesh-like structure, we notably faced difficulty measuring the surface roughness through AFM. This was because the cantilever tip got trapped, resulting in an erroneous measurement. Therefore, we were unable to measure the P-L mat. Due to the random distribution of P-L flakes inside the scaffold, the surface exhibited a high crest; as a result, the surface roughness (Sq) of the P-L flakes was found highest with values of 275.21 nm when observed from 3D surface images; whereas the surface roughness of the P-L powder and PDMS (P) alone was observed relatively lower, i.e., 145.18 nm and 5.208 nm, respectively (Table 4.3).

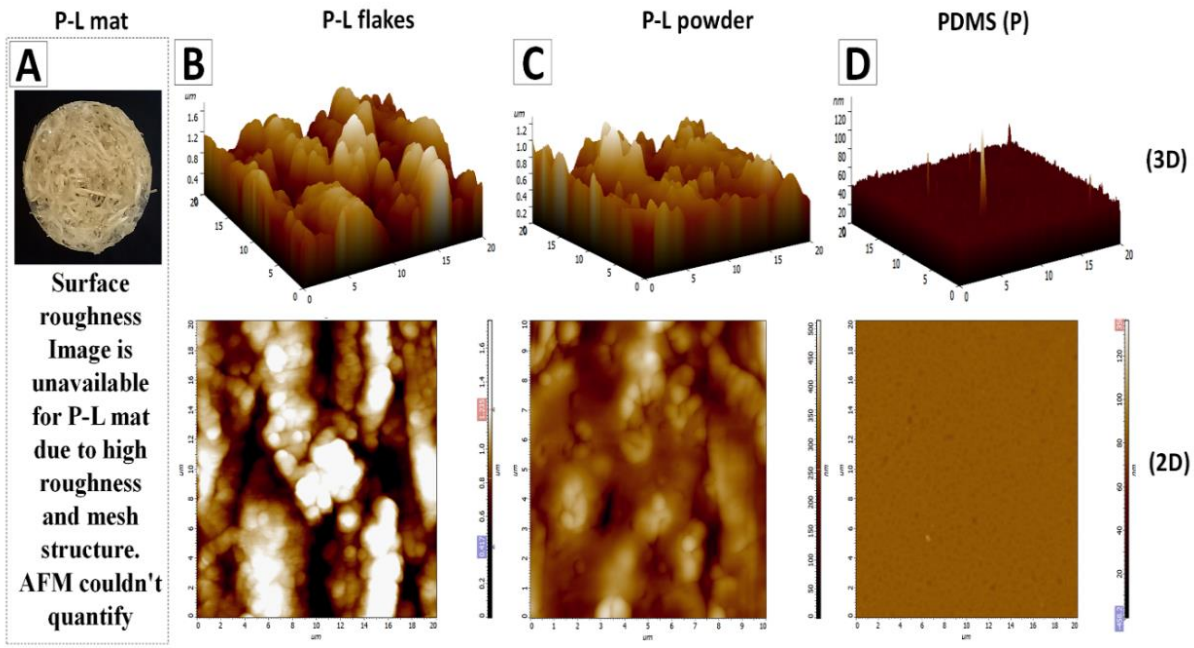

Figure 4.4: Represents the (A) digital image of P-L mat, and surface roughness analysis measured by atomic force microscopy (AFM) in 3D and 2D of (B) P-L flakes, (C) P-L powder, and (D) PDMS (P) scaffolds to justify their surface roughness.

Table 4.3: Represents surface roughness parameters of scaffold P-L flakes, P-L powder, and PDMS (P) in 3D measured using Atomic force microscopy (AFM). Data were analyzed using One-way ANOVA Tukey's Post hoc Test.

Scaffold name	Root mean square roughness (Sq)	Average roughness (Sa)	Area peak to valley height (St)	Highest peak height (Sp)	Maximum area valley depth (Sv)	Sampling area (As)
P-L flakes	275.21 nm	218.41nm	1762.5 nm	846.6 nm	915.8 nm	400 µm ^{2}
P-L powder	145.18 nm	110.99 nm	1290.6 nm	612.3 nm	678.2 nm	400 µm ^{2}
PDMS (P)	5.208 nm	3.852 nm	136.16 nm	95.95 nm	40.21 nm	400 µm ^{2}

4.3.1.3 Determination of effective porosity of the scaffold

The effective porosity of the samples was also quantified using the solvent replacement technique, as defined previously (Gundu et al. 2022). The effective porosity of P-L mat, P-L flakes, P-L powder and PDMS (P) was estimated to be 14.63 ± 3.69%, 20.72 ± 6.43%, 10.08 ± 2.68%, and 4.04 ± 1.87%, respectively. The highest and lowest weight gain was observed in P-L flakes (20.72 ± 6.43%) and PDMS (P) (4.04 ± 1.87%) scaffolds, respectively (Figure 4.5). The degree of porosity was found to be significantly lower in P-L powder and PDMS (P) than in P-L mat and P-L flakes. This was most likely due to the lack of pores in the PDMS scaffold and densely packed luffa powder microstructure and PDMS, resulting in less porosity than that of P-L flakes.

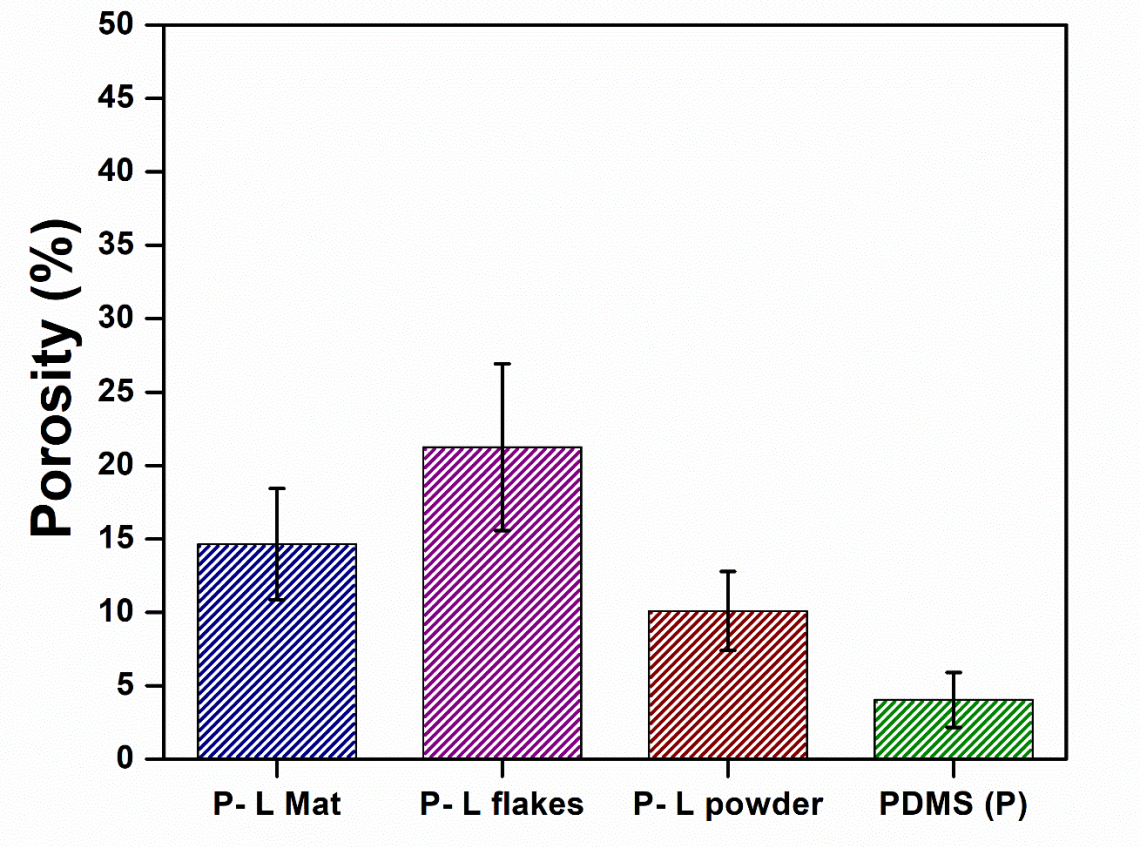

Figure 4.5: Graph depicts the effective porosities of P-L mat, P-L flakes, P-L powder, and PDMS (P) scaffolds. The effective porosities were calculated using the ethanol replacement method.

4.3.1.4 Thermogravimetric analysis (TGA)

The thermogravimetric analysis (TGA) of cured P-L mat, P-L flakes, P-L powder, and PDMS (P) is shown in Figure 4.6. The initial weight loss (1.2%) up to 200^{o}C in P-L powder and P-L flakes were observed, most likely due to the desorption of water molecules, which was absent in PDMS (P) and P-L mat. The cured PDMS (P) showed a one-step degradation of 235-675^{o}C, depicting the loss of organic groups. The total weight loss percentage shown by cured PDMS (P) was 54% indicating a high silicon content. P-L mat showed a similar but higher weight loss percentage (59%) compared to PDMS (P) due to the luffa component. This weight loss depicted a very small amount of luffa in the P-L mat. Both P-L powder and P-L flakes showed two weight loss steps, viz. 235- 400^{o}C and 400- 657^{o}C for P-L flakes, and 235-425^{o}C and 425-670^{o}C in the case of P-L powder, respectively, indicating the presence of a high percentage of

luffa in the form of powder or flakes. The total weight loss percentage in P-L powder and P-L flakes was 81% and 75%, respectively.

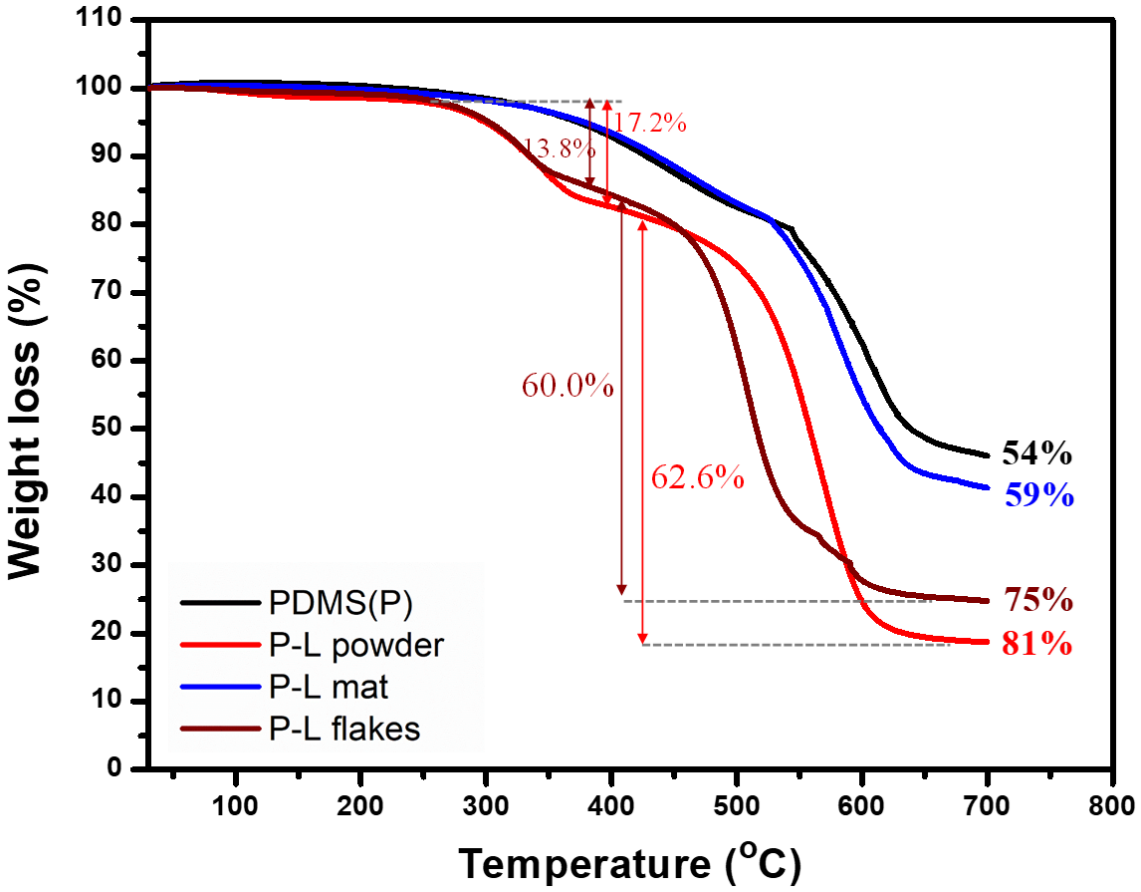

Figure 4.6: Thermogravimetric analysis (TGA) graph for P-L mat, P-L flakes, P-L powder and PDMS (P) scaffolds.

4.3.1.5 Surface wettability measurement

The surface wettability defines the degree of hydrophilicity and hydrophobicity of the scaffolds. The ImageJ technique was used to quantify the liquid contact angle to evaluate the wettability and hydrophilic properties. Based on the contact angle values, the surface area can be categorized as hydrophobic (contact angle > 90°) or hydrophilic (contact angle < 90°). Immediately after the drop was deposited, i.e., at time t = 0, all scaffolds were observed less hydrophilic. After 30 and 60 minutes of incubation, the contact angle on the surfaces of luffa-containing scaffolds began to decrease, indicating hydrophilic behavior. At t=0, all the

scaffolds exhibited contact angles in the 100-120 degree (°), indicating less hydrophilic behavior. After 30 minutes, the contact angle of the P-L mat, P-L flakes, and P-L powder were reduced to 50.64 ± 4.19°, 78.52 ± 4.15°, and 84.30 ± 3.95°, respectively. After 90 minutes, the contact angle values for luffa-containing scaffolds, i.e., P-L mat, P-L flakes and P-L powder, were further reduced to 19.08 ± 3.03°, 29.69 ± 3.59° and 50.67 ± 3.73°, respectively. Contact angles at various time intervals can be seen in Table 4.4. The contact angle of PDMS (P) showed the least changes due to the hydrophobic behavior of the scaffolds. The slight decrease in the contact angle values may be observed due to gravity and liquid evaporation from the surrounding environment (Figure 4.7).

Table 4.4: Surface water contact angle values (^{o}) of various forms of luffa-PDMS-based scaffolds measured at 0, 30, 60, and 90 minutes time intervals. Data were analyzed using One-way ANOVA Tukey's Post hoc Test.

S.No.	Name	0 min	30 min	60 min	90 min
1.	P-L mat	112.90 ± 5.65	50.64 ± 4.19	39.06 ± 4.22	19.08 ± 3.03
2.	P-L flakes	117.88 ± 5.83	78.52 ± 4.15	56.43 ± 3.47	29.69 ± 3.59
3.	P-L powder	117.12 ± 7.32	84.30 ± 3.95	65.47 ± 5.62	50.67 ± 3.73
4.	PDMS(P)	100.93 ± 4.70	94.52 ± 3.57	85.82 ± 3.69	76.34 ± 2.21

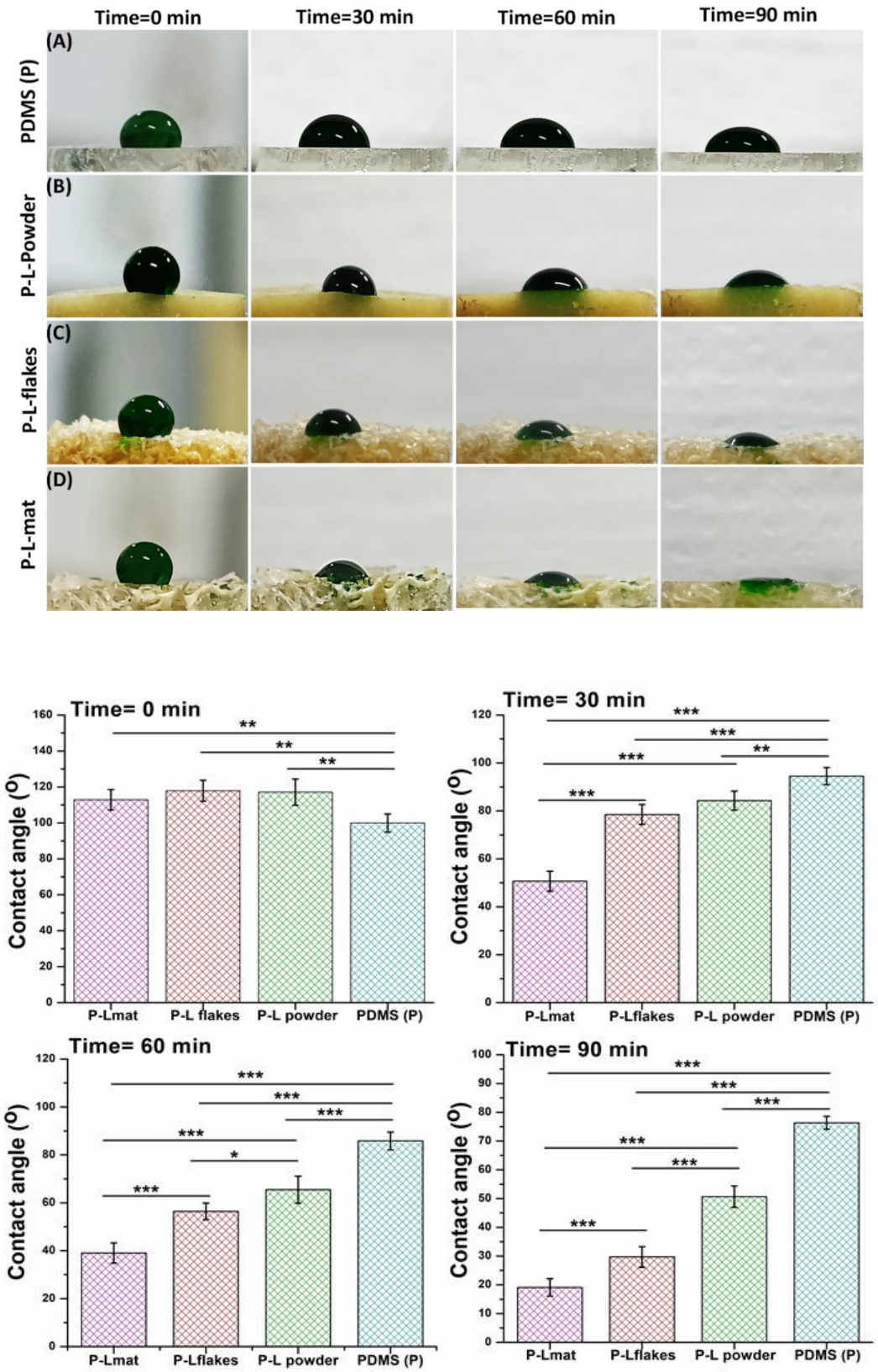

Figure 4.7: Time-dependent contact angle of various forms of luffa-PDMS-based scaffolds at 0, 30, 60, and 90 min time intervals.

4.3.1.6 Efficiency of the scaffolds to absorb oil, PBS and organic solvents

The porosity defines the liquid retention capacity of the scaffolds; however, the scaffold's swelling percentage determines its liquid absorption ability. Weight gain percentage was found to be 13.54 ± 1.79%, 20.45 ± 2.84%, 12.48 ± 0.55%, 2.22 ± 0.38%, 30.26 ± 4.73% for motor oil and 24.29 ± 1.36%, 29.56 ± 5.16%, 20.95 ± 0.15%, 1.74 ± 0.16%, 39.70 ± 2.65% for phosphate buffer solution (PBS) in case of P-L mat, P-L flakes, P-L powder, PDMS (P) and L mat scaffolds, respectively (Table 4.5), as shown in Figure 4.8. We have examined the absorption of different crude oil micro and macro components with the fabricated scaffolds, including oil, toluene, n-hexane, cyclohexane, and other chemical components like diethyl ether.

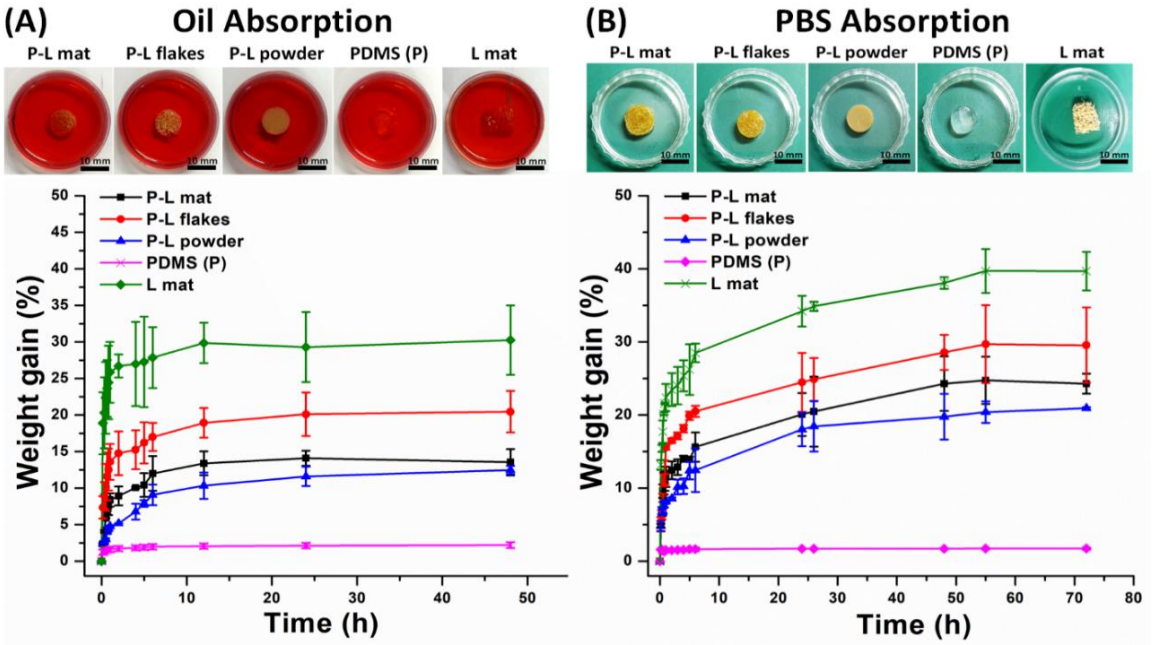

Figure 4.8: Digital images depict (A) oil absorption study with respective weight gain plots, (B) PBS absorption with respective plots; P-L mat, (B) P-L flakes, (C) P-L powder, (D) PDMS (P) and (E) L-mat scaffolds.

Table 4.5: The absorption efficacy (%) of the fabricated scaffold when placed in PBS and oil. Data were analyzed using One-way ANOVA Tukey's Post hoc Test.

S.No.	Name	Oil absorption (%)	PBS absorption (%)
1.	P-L mat	13.54 ± 1.79	25.79 ± 2.06
2.	P-L flakes	20.45 ± 2.84	33.30 ± 1.27
3.	P-L powder	12.48 ± 0.55	21.45 ± 0.55
4.	PDMS(P)	2.22 ± 0.38	1.72 ± 0.04
5.	L mat	28.34 ± 3.61	38.23 ± 1.72

For P-L mat, P-L flakes, P-L powder, PDMS (P) and L mat, the weight gain for toluene was 104.86 ± 5.10%, 126.14 ± 5.08%, 91.83 ± 3.61%, 155.18 ± 9.86% and 86.18 ± 16.92%, respectively. Similarly, for cyclohexane and n-hexane, the values were observed as 108.40 ± 5.48%, 127.37 ± 2.53%, 92.80 ± 4.25%, 160.95 ± 7.98%, 47.09 ± 9.41% and 97.27 ± 1.54%, 133.03 ± 3.71%, 91.80 ± 0.37%, 113.21 ± 3.90%, 29.36 ± 3.39% for P-L mat, P-L flakes, P-L powder, PDMS (P) and L mat, respectively (Table 4.6). Although diethyl ether is not a constituent of crude oil, we have examined it and noticed an increment in its absorption. The weight gain percentage of P-L mat, P-L flakes, P-L powder, PDMS (P), and L-mat using diethyl ether was found to be 86.69 ± 1.95%, 128.05 ± 7.97%, 90.03 ± 2.91%, 97.32 ± 5.44%, and 30.13 ± 0.15%, respectively. PDMS (P) showed the highest absorption for toluene (155.18 ± 9.86%) and cyclohexane (160.95 ± 7.98%) whereas P-L flakes demonstrated the highest absorption for n-hexane (133.03 ± 3.71%) and diethyl ether (128.05 ± 7.97%) (Figure 4.9).

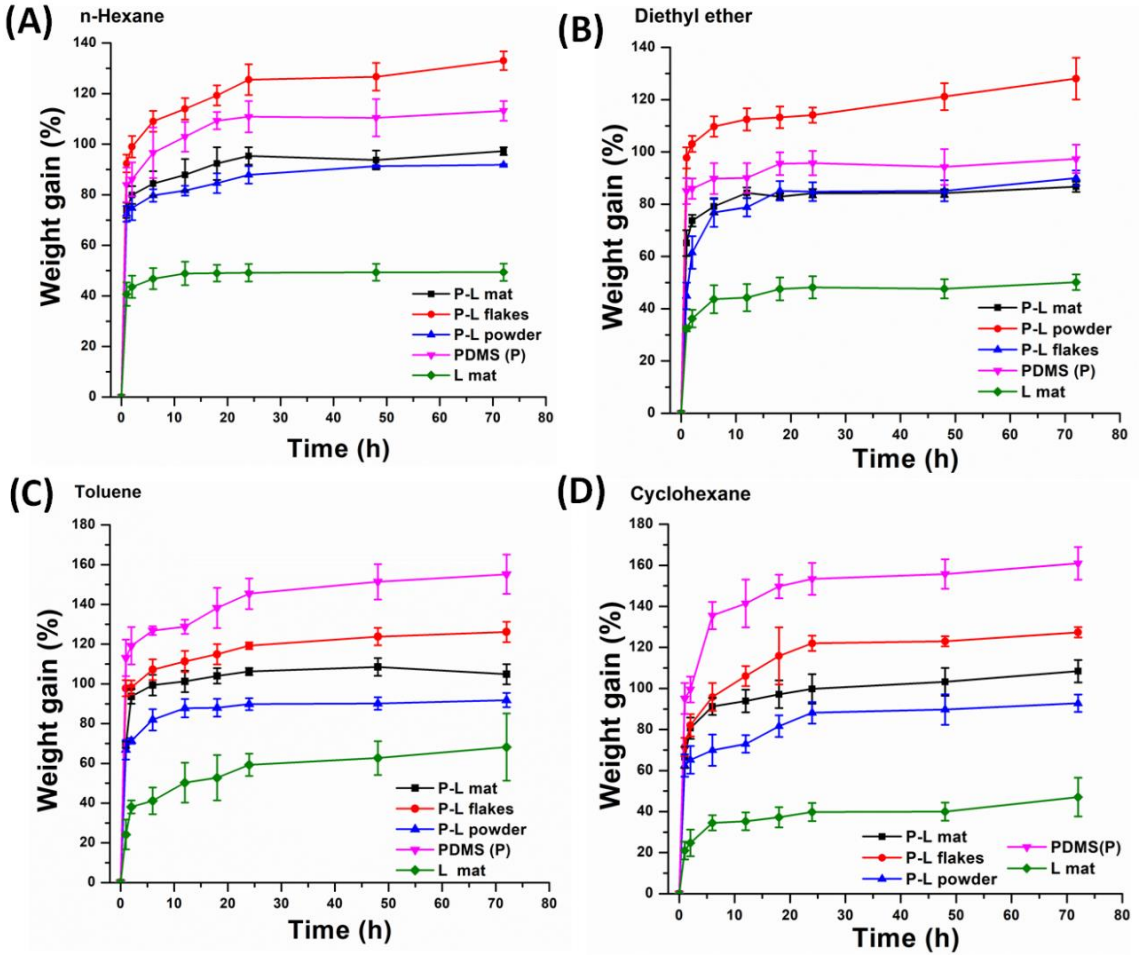

Figure 4.9: Graphical representation of changes in weight gain percentages over time in organic solvents (A) n-hexane, (B) diethyl ether, (C) toluene, and (D) cyclohexane.

Table 4.6: The absorption efficacy (%) of the fabricated scaffold's when placed in organic solvents. Data were analyzed using One-way ANOVA Tukey's Post hoc Test.

S.No.	Name	Toluene (C_7H_8)	Cyclohexane (C_6H_{12})	n-hexane (C_6H_{14})	Diethyl ether ($C_4H_{10}O$)
1.	P-L mat	104.86 ± 5.10	108.40 ± 5.48	97.27 ± 1.54	86.69 ± 1.95
2.	P-L flakes	126.14 ± 5.08	127.37 ± 2.53	133.03 ± 3.71	128.05 ± 7.97
3.	P-L powder	91.83 ± 3.61	92.80 ± 4.25	91.80 ± 0.37	90.03 ± 2.91
4.	PDMS(P)	155.18 ± 9.86	160.95 ± 7.98	113.21 ± 3.90	97.32 ± 5.44
5.	L mat	86.18 ± 16.92	47.09 ± 9.41	29.36 ± 3.39	30.13 ± 0.15

4.3.1.7 Oil-Water sorption study

In a glass beaker (Borosil) with a 25 mL capacity, oil spill absorption was established by adding 1 mL of oil to 15 mL of water. This was performed to assess the behavior of the sorbent materials in terms of their ability to absorb oil and acquire weight gain. Motor oil has been used to replicate the oil transportation process. Evaluation of oil-water sorption was quantified by measuring the weight gain at physiological temperature (37ºC). The weight of water gain was negated as described in the method section. Table 4.7 shows the weight gain from the sorption of the oil-water mixture was found to be 16.09 ± 4.62%, 24.49 ± 3.56%, 15.52 ± 2.67%, 5.52 ± 1.44% and 34.31 ± 4.02% for P-L mat, P-L flakes, P-L powder, PDMS (P) and L-mat, respectively. Since luffa exhibits oleophilic nature, L-mat exhibited maximum oil-water absorption. PDMS (P) showed neutral behavior towards oil absorption, i.e., it does not absorb any significant level of oil-water as such. Figure 4.10 shows the weight gain percentage of the scaffolds and Figure 4.11 represents the digital images of oil sorption study.

Table 4.7: Weight gain of scaffold from oil-water mixture. Data were analyzed using One-way ANOVA Tukey's Post hoc Test.

S.No	Scaffold name	Oil sorption (%)
1.	P-L mat	16.09 ± 4.62
2.	P-L flakes	24.49 ± 3.55
3.	P-L powder	15.52 ± 2.67
4.	PDMS(P)	5.52 ± 1.44
5.	L-mat	34.31 ± 4.0

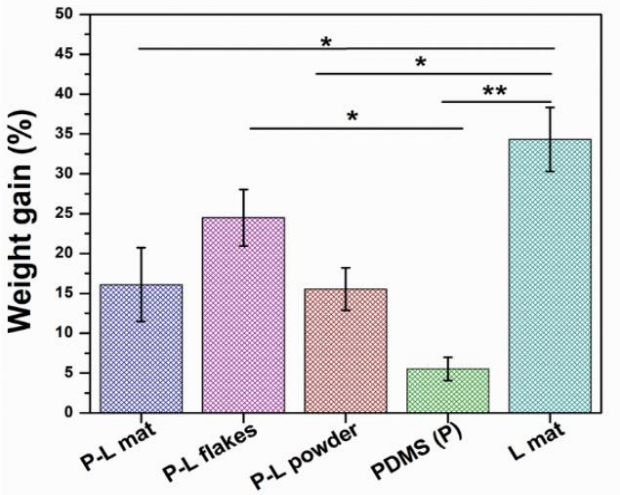

Figure 4.10: Graphical representation of the weight gain percentages of various scaffolds.

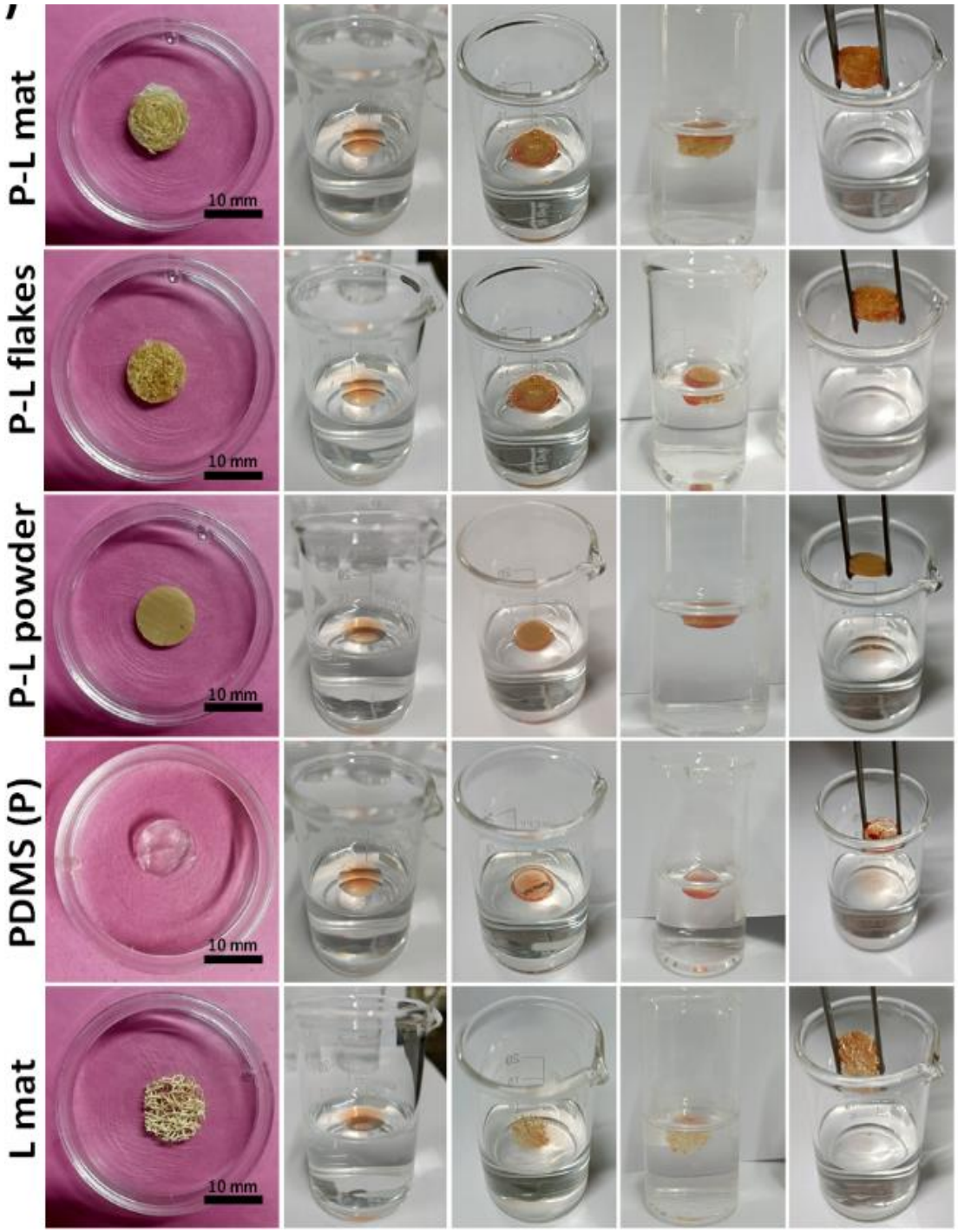

Figure 4.11: Digital images depict the oil sorption study of P-L mat, P-L flakes, P-L powder, PDMS (P), and L-mat scaffolds.

4.3.1.8 Reusability of fabricated scaffolds

The fluorescent microscopic images depict the cytocompatibility of MG-63 osteoblast-like cells cultured for 2, 4, and 6 days on the fabricated three-dimensional composite scaffolds i.e., 3% LC, 5% LC and control (C). The results revealed improved cellular biocompatibility and adequate proliferation of MG-63 osteoblast-like cells. We attempted to reuse the material by using the thermal desorption technique. The process involved soaking the oil of the scaffold using tissue paper, then washing it in hot water and drying it at 60^{o}C for 30 minutes. By adopting this approach, the scaffold was effectively recovered, and its absorbent capacity was restored. We monitored the recovery process 10–12 times and found that the scaffold's effectiveness decreased by 10% after 10–12 times due to a lack of recovery following multiple washes. However, successful scaffold recovery offers the prospect of environmentally sustainable reuse. We anticipate that the solvent extraction approach would be better suited for recovering absorbed/adsorbed oil and reusing our scaffold. Furthermore, the outcomes suggest that the fabricated scaffold can be reused a few times; however, it may not require repeated usage because the materials involved are readily available, inexpensive, and environmentally benign. The byproduct components may be repurposed for various other applications.

4.3.1.9 Assessment of mechanical stability

Compressive and tensile testing's were performed for all the fabricated scaffolds to measure their mechanical stability. Figure 4.12 (A) illustrates the compressive stability of all scaffolds. The compressive Young's modulus of P-L mat, P-L flakes, P-L powder and PDMS (P) was found to be 21.04 MPa, 4.68 MPa, 3.46 MPa, and 2.38 MPa, respectively, and the compressive strength was estimated to be 3.70 MPa, 2.37 MPa, 14.72 MPa and 8.95 MPa, respectively. The tensile graph (Figure 4.12(B)) was obtained by plotting tensile stress against strain values. The Young's modulus of the P-L mat, P-L flakes, P-L powder and PDMS (P) was evaluated as

20.72 MPa, 4.00 MPa, 2.15 MPa, and 1.72 MPa, respectively, and tensile strength was assessed as 1.66 MPa, 0.20 MPa, 0.51 MPa, and 0.37 MPa, respectively (Table 4.8).

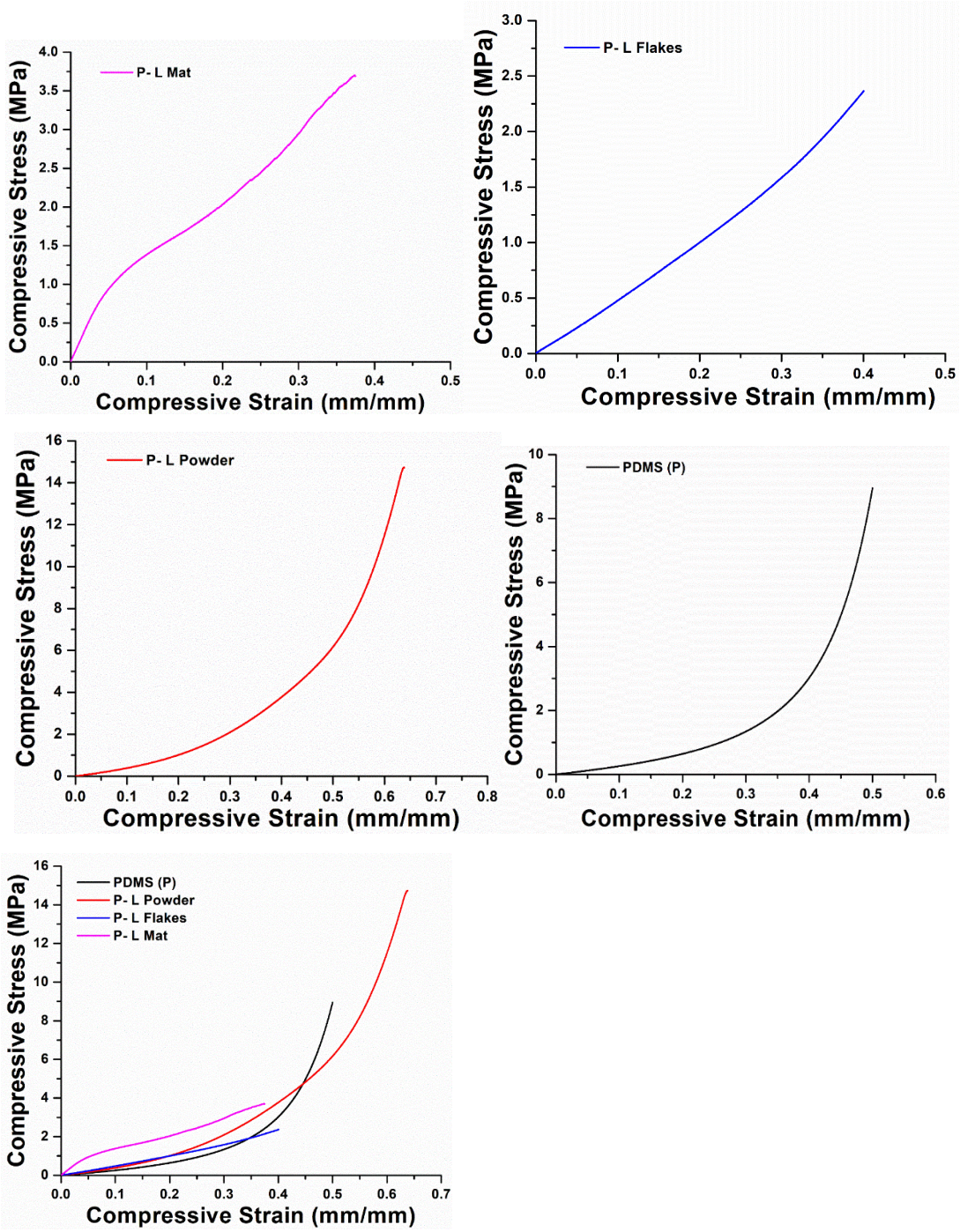

Figure 4.12 (A): Graph shows compressive stability of various scaffolds.

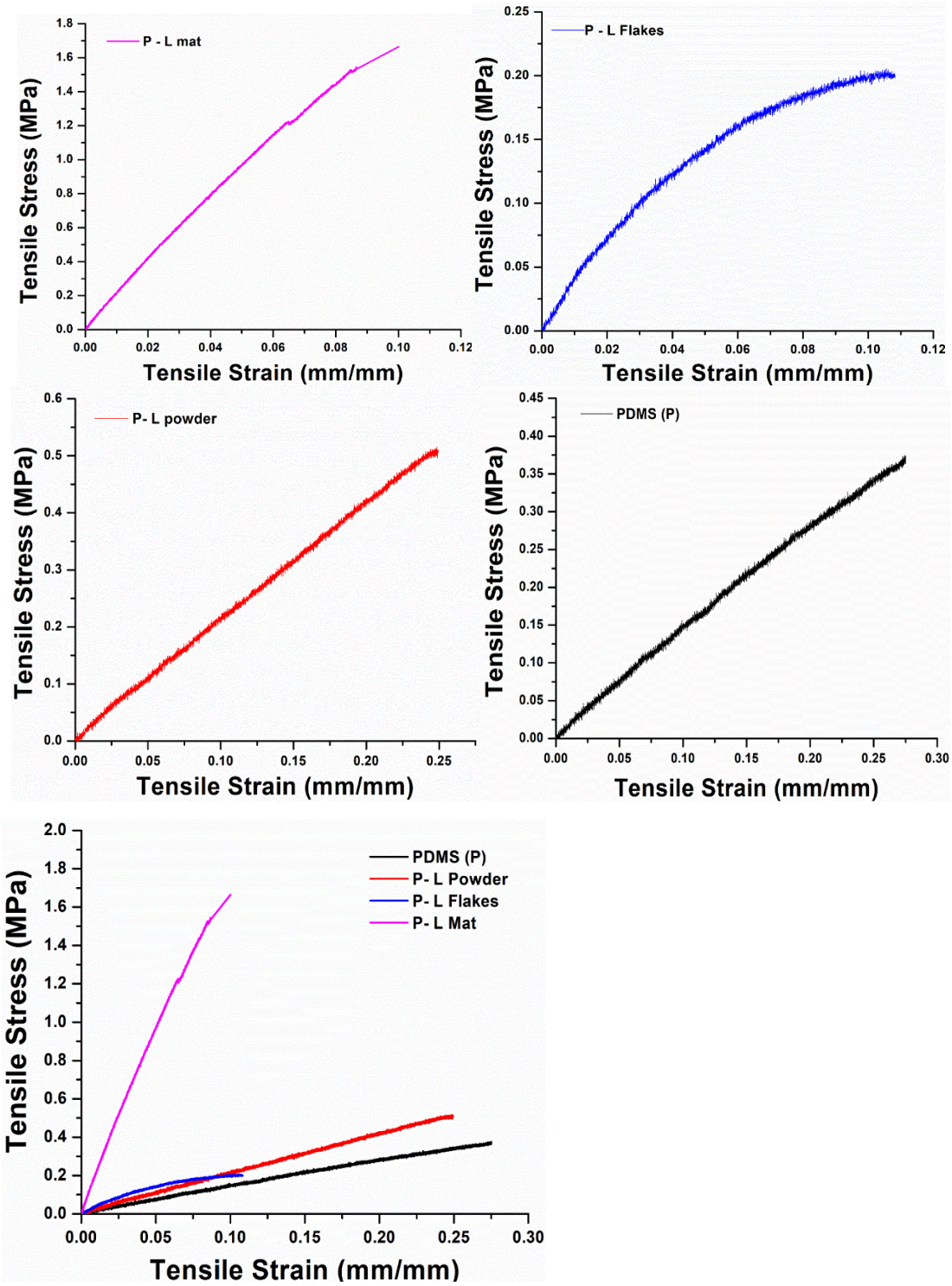

Figure 4.12 (B): Graph shows tensile stress-strain curve until breakpoint of various scaffolds.

Table 4.8: Mechanical properties showing young's modulus and strength of scaffolds. Data were analyzed using One-way ANOVA Tukey's Post hoc Test.

	Compressive parameters			Tensile parameters		
S.No.	**Name**	**Young's modulus (MPa)**	**Compression strength (MPa)**	**Young's modulus (MPa)**	**Tensile strength (MPa)**	**Break point**
1.	P-L mat	21.04	3.70	20.72	1.66	0.10
2.	P-L flakes	4.68	2.37	4.00	0.20	0.11
3.	P-L powder	3.46	14.72	2.15	0.51	0.25
4.	PDMS(P)	2.38	8.95	1.72	0.37	0.27

4.3.1.10 Cell cytotoxicity study:

A significant improvement in cellular viability was noticed over the course of a 4-day culture on plasma-treated P-L mat, P-L flakes, P-L powder, and PDMS (P) scaffolds for MG-63 (human bone osteoblast) cells (Figure 4.13). Cells cultured on 96-well plates were considered as the control, and the rest of the values were quantified relative to the control. All the scaffolds exhibited a significant enhancement in the proliferation percentage of MG-63 cells from 35.36 ± 2.70%, 31.98 ± 1.56%, 33.92 ± 2.07%, 29.09 ± 3.40% observed on the second day of culture to 51.12 ± 3.14%, 54.40 ± 2.29% and 39.88 ± 2.85% by the fourth day of culture for control PDMS (P), P-L powder, P-L flakes, and P-L mat, respectively.

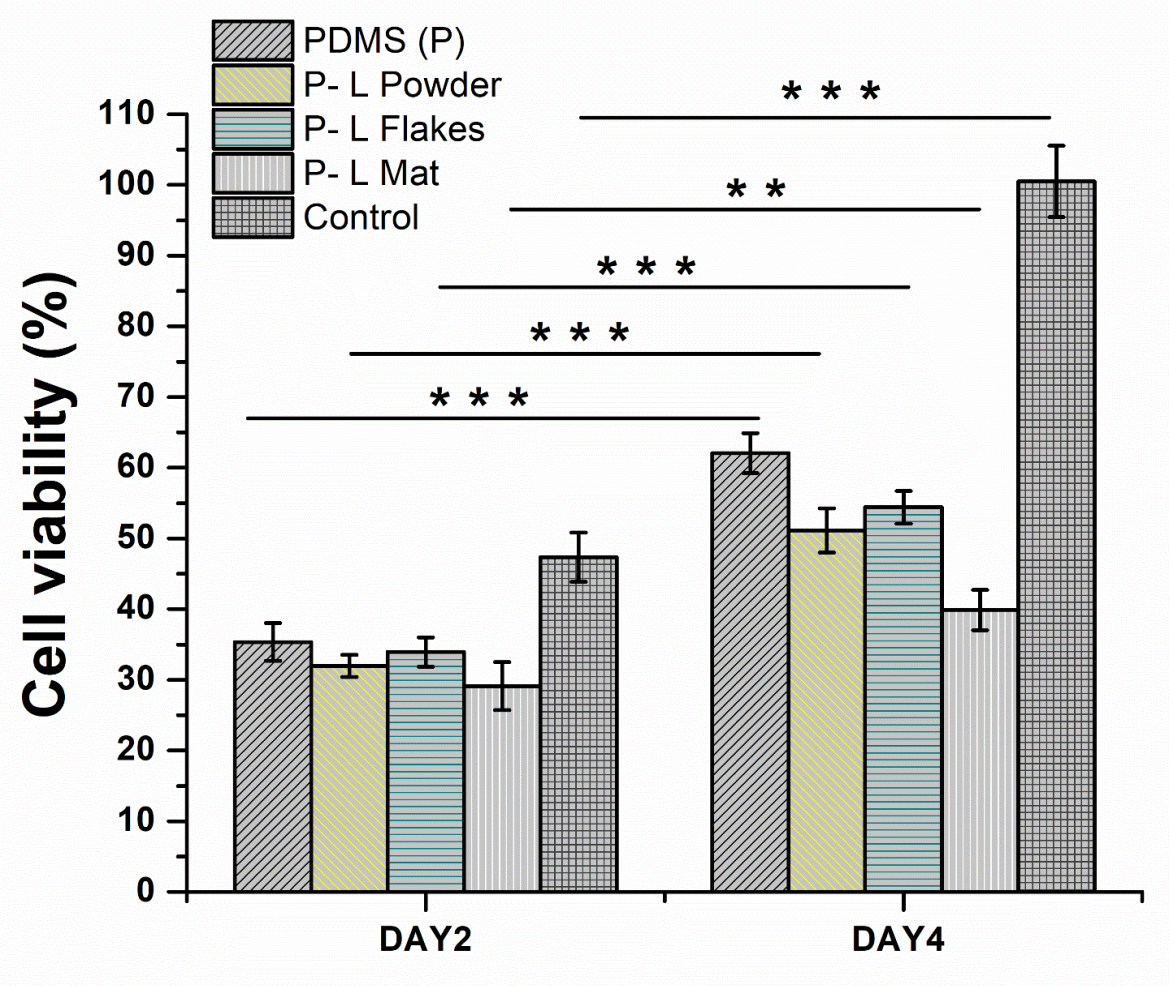

Figure 4.13: Graph represents the percentage cellular viability of MG-63 (Human osteoblast) cells. The 4th-day control was considered a positive control and its OD was considered reference OD for all the samples. Data were analyzed using One-way ANOVA Tukey's Post hoc Test. Values are expressed as mean ± SD (n=6) and the level of significance as *p<0.05, **p<0.01, and ***p<0.001, respectively.

4.3.1.11 Biodegradation of the scaffold

A degradation study was carried out to understand the change in morphology and weight loss of the scaffolds when treated with enzymes such as lysozyme. Biodegradation assessment is essential to verify the stability of fabricated materials under harsh conditions. For biodegradation tests, scaffolds of 10 mm diameter were submerged in a lysozyme solution with continuous stirring for 20 days of incubation. The results revealed that all the scaffolds were almost stable, and no substantial degradation was noticed physically. However, some level of

weight reduction was observed when the final weights of scaffolds were compared with their initial values, as shown in Figure 4.14. Figure 4.14 graph shows that P-L flakes exhibited noticeably higher weight loss (i.e., 3.64 ± 0.40%) when compared to the other scaffolds; most likely due to the presence of the high amount of microcapillaries within the luffa that got exposed to lysozyme degradation. The scaffolds P-L mat, P-L flakes, P-L powder and PDMS (P) have shown weight loss percentages of 2.72 ± 0.90%, 3.64 ± 0.40%, 2.40 ± 0.82%, and 1.80 ± 0.24%, respectively.

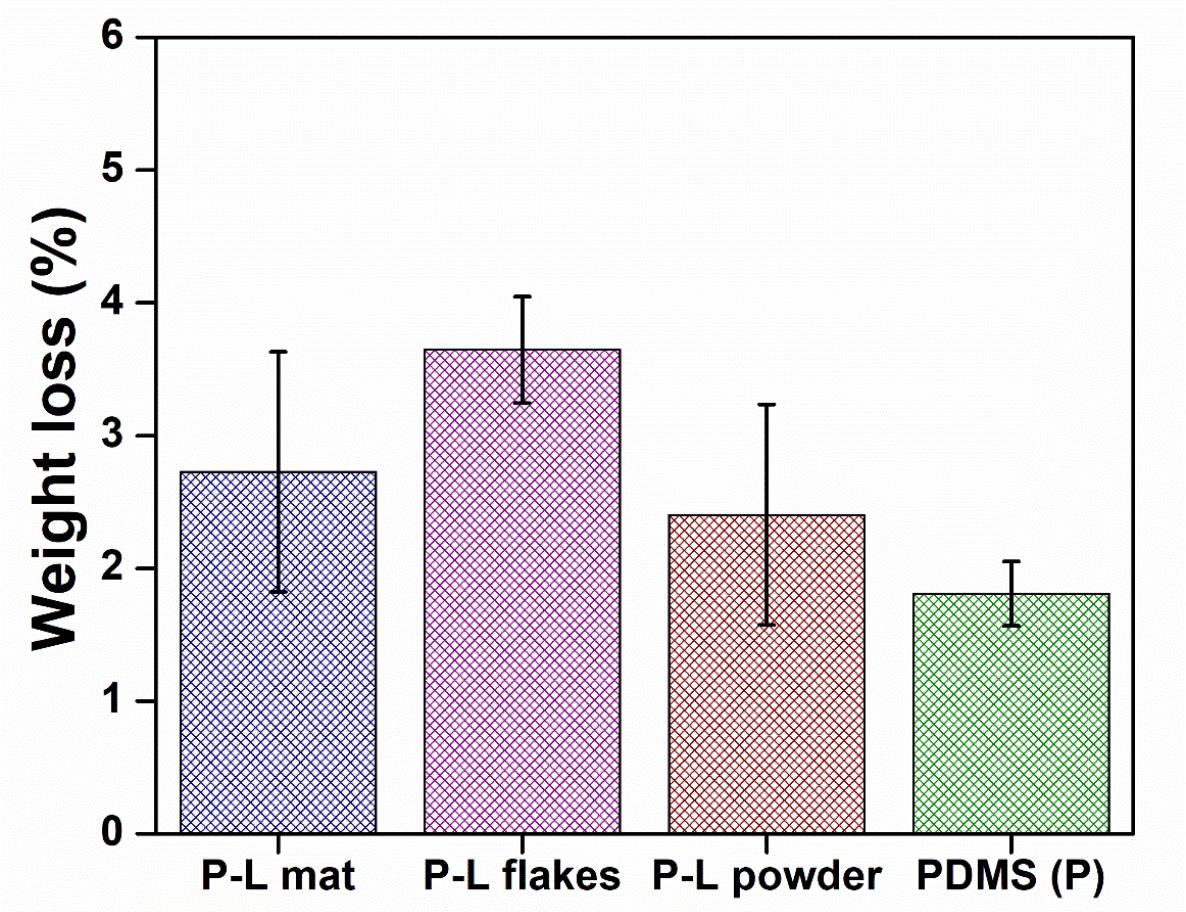

Figure 4.14: Graph represents the in vitro degradation of P-L mat, P-L flakes, P-L powder, and PDMS (P) scaffolds after 20 days in a lysozyme-containing solution at 40^{o}C. One-way ANOVA Tukey's Post hoc Test was performed, and the values are expressed as mean ± SD (*n*=3).

4.4 Discussion

Several previous reports have claimed LC to be one of the potential candidates for the sorption of oil spillage, biodegradability, recyclability, cost-effective and eco-friendly characteristics (Menya et al. 2018; V. Singh et al. 2014; Z. Wang et al. 2017). LC alone is more susceptible to sink because of low hydrophobicity and highly porous structure; it experiences low buoyancy forces. As a result, polydimethylsiloxane (PDMS) was utilized as a hydrophobic material that was designed to associate with LC and further support LC for enabling it to serve as a highly floatable scaffold in the process of oil-water separation. As a result of the high flexibility, thermal stability, and hydrophobicity of PDMS, the water barely penetrates PDMS, which prevents the PDMS-impregnated LC scaffold from sinking into water (Laitinen et al. 2017; C. Yu et al. 2017). Moreover, PDMS, a silicone-based organic polymer, appears as a promising floating substrate due to its intrinsic transparency, mechanical flexibility, weather resistance, and environmental non-toxicity (Park and Hur 2021). According to Kim et al., the hydrophobic, lighter weight, and immiscible properties of PDMS enable it to float on the water's surface (Kim, Kim, and Park 2019). Moreover, reports have claimed that thin layers of PDMS have the advantage of gaseous permeability that would not prevent the gaseous exchange between air and water bodies leading to no harm to aquatic creatures (Lamberti, L. Marasso, and Cocuzza 2014; Markov et al. 2014). Several prior reports have shown the advantages and applications of luffa structure in various forms for oil spillage studies. Luffa comprises a fibrous network structure with greater absorption capability that can be utilized as a very effective oil- absorbing material by altering the surface. Studies on oil absorption, performed by Wang et al. via fabricating porous luffa sponge, revealed that porous structure LC can absorb oils up to 8 to 12 times its weight (Z. Wang et al. 2017). Water absorption in cellulose fibers is caused by hydrogen bonding between free hydroxyl groups on cellulose molecules and water molecules. Luffa, when poorly bound with other composite material and

processed with surface modification, results in cracks and voids between the polymer matrix and luffa fiber leading to easy penetration and storage of water/liquid through the voids (Demir et al. 2006). Composite materials exhibit functions better than the conventional materials when immersed in water and exposed to wind, rain, and sun. However, structural degradation can cause unanticipated structural failures with these materials. These factors should be considered while designing such construction. Examining the performance of natural fiber-based polymer composites in terms of water absorption is crucial to their end-use applications. Water absorption may degrade some qualities; thus it should be considered when choosing its certain application (Seki et al. 2012). Yu M. et al. claimed a modular, ecologically safe, and low-cost dip coating method to improve the commercial luffa sponge with aqueous polyurea and fused SiO_2 nanoparticles to create a super hydrophobic sponge without harmful low-surface-energy compounds. Due to its great chemical stability, the as-prepared luffa sponge had good super hydrophobic/ super oleophilic qualities and was found resilient for oil-water separation in hostile settings and extremely harsh conditions. The produced luffa sponge exhibited outstanding anti-fouling, self-cleaning, and surfactant-free oil-in-water emulsion absorption. More crucially, after more than 50 abrasion cycles, the as-prepared luffa sponge retained its super hydrophobicity and oil/water separation efficiency (M. Yu et al. 2018).

Through our research efforts, we envisioned observing the ability of various forms of luffa in combination with PDMS to absorb oils and other organic solvents. The scaffolds were fabricated using the hand lay-up method. The fabricated scaffolds were subjected to various characterizations such as scanning electron microscopy analysis, atomic force microscopy, porosity, organic solvent absorption, mechanical testing, and oil-water absorption analysis. Morphological analysis of the scaffolds calculated using the ImageJ software revealed the surface roughness of several forms of luffa. PDMS without any luffa appeared smoother with negligible peaks, although a few visible peaks were observed because of dust or foreign

particles. P-L powder exhibited the highest number of sharp peaks evenly distributed on its surface. The surface of P-L mat displayed a broader peak with fewer numbers in a non-continuous manner. P-L flake scaffolds exhibited coarsely chopped fibers with an average number of peaks having uneven distribution. The surface area of P-L powder was found to be the highest among all the scaffolds, probably because of the highest number of peaks. From Figure 4.2, we have analyzed the internal 3D architecture of the scaffolds. SEM images of the P-L mat (Figure 4.3) revealed the luffa fibers embedded within the PDMS; displaying its microcapillaries and microporous structures. While the luffa fibers were present throughout the scaffold in the P-L mat, they were observed sparsely distributed in the P-L flakes scaffold; whereas luffa flakes were found randomly arranged within PDMS. The P-L flakes scaffold exhibited a high density of luffa microparticles, resulting in a high surface area-to-volume ratio and superior oil absorption compared to the other scaffolds. Also, the fragmented flakes of luffa are believed to be distributed throughout the P-L flakes scaffold mimicking the continuously accessible and interconnected capillary arrangement enabling it for the highest oil absorption efficiency. However, the P-L powder, which had a fine micron size, was compactly packed within the PDMS and due to the lack of capillaries-like architecture, it appeared as an agglomerated material that was also distinctly visible at different magnifications when observed through SEM. Therefore, in P-L powder scaffolds, luffa particles incorporated within PDMS were largely inaccessible and non-interconnected. The digital images demonstrate the 3D architecture of the scaffold. In addition, the surface roughness of the scaffolds was examined using a conventional characterization technique atomic force microscopy (AFM). The data demonstrate that the surface roughness quantification could not be accomplished in the case of P-L mat because of the high crest and trough network that hindered the cantilever tip movement. In P-L flakes, P-L powder, and PDMS scaffolds, surface roughness was quantified and compared based on the 2D and 3D topographical images. From

the topographical analysis, we observed that the P-L flakes scaffold had the highest surface roughness, resulting in a higher surface area-to-volume ratio, with greater peak frequencies and larger crests. Conversely, the P-L powder exhibited a more densely packed structure, resulting in a significant loss of the microporous architecture, and therefore, the surface of the P-L powder exhibited fewer peaks and a lower frequency of crests. The PDMS scaffold appeared completely smooth, and any negligible peaks on the surface were observed, most likely due to the deposition of dust particles. The results obtained from AFM) were well agreed with the surface roughness observed through the ImageJ technique, as shown in Figure 4.2.

The effective porosity of the scaffolds was determined using the ethanol displacement method (Guan et al. 2005). Irrespective of the high surface area, the P-L powder scaffolds did not exhibit the highest porosity, this could be due to the involvement of only exposed luffa microparticles for permeating ethanol inside; while the rest of the luffa microparticles densely packed within the PDMS were perhaps enclosed by hydrophobic PDMS; preventing ethanol permeation. The highest ethanol permeation was found with P-L flakes because macroparticles of luffa resulted in a high amount of ethanol permeation because of many microcapillaries. P-L mat also permeated a good amount of ethanol; however, since the luffa particle was exposed notably less, the resulting effective porosity was lesser than that of P-L flakes. PDMS (P) scaffolds exhibited negligible pores, resulting in no ethanol uptake. Figure 4.15 depicts the digital and SEM micrographs of luffa flakes, which clearly show the microcapillaries of the flakes. Figure 4.15 (C) confirms the porous structure of the luffa flakes material, which exhibits luffa's hydrophilic and oleophilic properties.

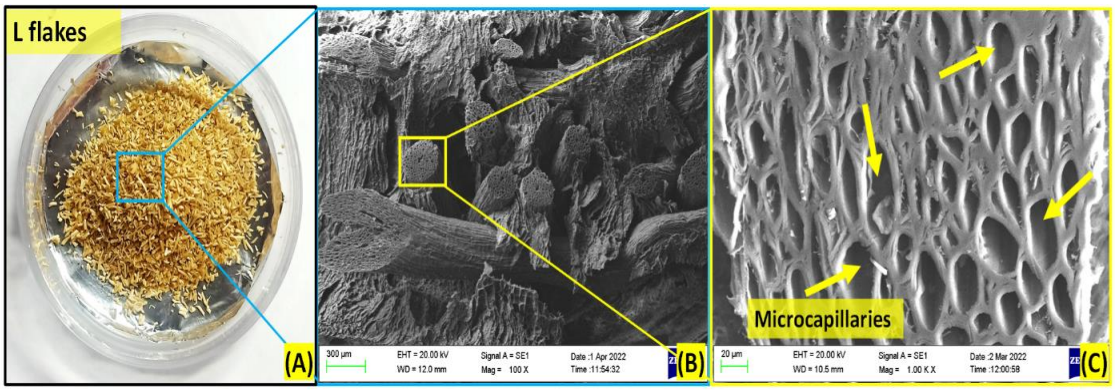

Figure 4.15: Illustrates the (A) digital image of luffa flakes (L flakes), (B) SEM micrographs at 100 x magnification, and (C) 1000 x magnification showing microcapillaries of luffa flakes.

The weight gain percentage of scaffolds in PBS, oil, and organic solvents was evaluated to examine the absorption capacity of the scaffolds. Weight gain of water and oil followed a similar trend for ethanol absorption due to the capillary effect. P-L flakes unveiled maximum weight gain percentage compared to their other respective forms. PDMS (P) showed the least weight gain percentage, as it was found unaffected (due to its hydrophobic nature) due to water and oil. The weight gain percentage of scaffolds in organic solvents resulted in variable trends based on the weight gain percentage of both luffa and PDMS. In addition, crude oil is composed of a wide variety of additional toxic components that have the propensity to be hazardous to aquatic life. Therefore, the absorption of particular organic compounds is of the utmost importance when dealing with oil spillage. Using n-hexane, cyclohexane, toluene and diethyl ether, PDMS (P) scaffolds exhibited the highest weight gain percentage compared to other scaffolds. The results have shown that PDMS (P) scaffold significantly absorbs certain toxic organic compounds. In addition, a comparison study is represented in Table 4.9 to show the efficacy of our fabricated scaffolds with other reported work utilizing similar or different materials and oils. We can deduce that different combinations of materials reported for oil-water separation applications exhibit noticeably varying results. Silicon-modified polyester materials fabricated using the chemical vapor deposition technique have exhibited superior

hydrophobicity and good separation efficiencies even after multiple recycling processes (Mao et al. 2023; J. Zhang and Seeger 2011). Wax coatings on natural sponges like luffa have improved the materials super-hydrophobicity and super-oleophilicity, leading to better separation efficiencies, absorption capacities, and simplified sample recycling (F. Wang, Lei, et al. 2019; F. Wang, Xie, et al. 2019). Modifying metallic meshes (for example, steel wool) by coating with PDMS has enhanced absorption rates and the potential to absorb relatively large amounts of oil (Abdulhussein, Kannarpady, and Biris 2019). Poly[(3,3,3-trifluoropropyl) methylsiloxane] PTFPMS-coated membranes stands out as an excellent oil-adsorbing material with good hydrophobicity even in extreme conditions like high temperatures, high humidity and corrosive environments (Hou et al. 2015). PDMS-coated polyvinylidene fluoride (PVDF) nanofibers fabricated via the electrospinning approach exhibit relatively shorter fabrication times with enhanced hydrophobicity and separation efficiencies (Cheng et al. 2021). Polybenzoxazine-modified cotton fabrics have demonstrated remarkable mechanical durability and good hydrophobicity enabling their usage even in adverse conditions (Bai et al. 2020; Shang et al. 2021). Inorganic nanoparticles applied to polyurethane foam have substantially increased its hydrophobicity and mechanical characteristics while expanding its application to various oils (H.-D. Liu et al. 2018). Polystyrene foams have improved oil adsorption capabilities and maintained their hydrophobicity even after several cycles, indicating their superior reusability (N. Zhang et al. 2017). Cellulose-based materials have demonstrated high separation efficiencies for various oils and are found robust in extreme circumstances such as high temperatures or low pH settings (Dan et al. 2020). The PDMS-functionalized melamine sponge has shown good large-scale oil absorption, exceptional absorption capabilities and great reusability, maximizing its utility in oil separation processes (Chen, Weibel, and Garimella 2016). However, these materials possess a few drawbacks, as listed in Table 4.9. While the reported scaffolds demonstrate promising features, several limitations still need to be

addressed. We have developed a novel scaffold to address the limitations of existing scaffolds. Our developed scaffold exhibits excellent oil absorption capacity, can withstand harsh conditions, allows for permeation of gaseous exchange, and prevents oxygen depletion in water. Additionally, super-hydrophobic behavior of the developed scaffolds enables it to remain floating and prevent sinking; rendering it a novel material for preventing oil spills. However, an improvement of the fabricated scaffolds to enhance the absorption percentage remains a scope for future research. The research study indicates that the fabricated luffa-PDMS scaffold is compatible with MG-63 osteoblast-like cells; indicating that the scaffolds are safe for use in oil spill treatment without affecting the marine ecosystem. For our upcoming experiments, we intend to expand the scope of our research by investigating additional cell lines such as MCF-7, HeLa, and NIH-3T3 to further explore the biocompatibility and potential applications of the scaffolds. This study will demonstrate our fabricated luffa-PDMS scaffold as highly compatible with a wide range of biological agents and without posing any potential toxicity hazards to marine life or the environment.

The surface wettability of the scaffolds was tested with all the scaffolds and it was found that almost all the scaffolds showed a contact angle higher than 90 degrees at the beginning; however, the contact angle started reducing for the scaffolds containing luffa w.r.t. time. PDMS (P) scaffold exhibited hydrophobic behavior throughout the time duration tested; only a slight reduction in the contact angle happened, which might be because of gravitational pull and evaporation of water molecules at the micro level. However, the P-L mat exhibited the lowest contact angle after 90 minutes, showing the high water absorption capacity of the P-L mat. However, the quantity studied for contact angle measurement was insufficient for determining the water permeation behavior.

Mechanical properties of scaffolds were tested based on their tensile and compressive strength. Among all the scaffolds, the compressive strength of P-L powder was found to be highest, i.e., 14.72 MPa; however, Young's modulus of P-L mat was found to be highest (21.04 MPa) among all the scaffolds. The result showed that PDMS (P) alone exhibited almost identical patterns to those of elastic materials. Incorporating evenly distributed luffa microparticles enhanced the compressive strength of the scaffold. The addition of luffa mat to the PDMS resulted in a noted reduction in the elasticity of the PDMS i.e., an increase in compression does not alter the change in strain proportionally. In the case of tensile strength, the P-L mat exhibited the highest tensile strength as well as Young's modulus in comparison to other forms of scaffolds. The main reason behind the non-elastic behavior of the P-L mat scaffold may be because of the high and continuous mesh network within the PDMS structure.

Oil-water absorption studies of the scaffold were quantified to check the efficacy of the fabricated scaffolds in terms of oil and organic solvent absorption capacity. The motor oil was used to perform absorption testing, and it was found that P-L flakes exhibited the highest oil absorption. Although PDMS surpassed in a few cases of organic solvent absorption, if we look forward to overall absorption capacity, P-L flakes outperformed in crude oil absorption and absorption of toxic organic solvents. Our investigations have demonstrated that luffa fibers preferentially absorb oil more efficiently than PBS, which is in accordance with a past study by Abdelwahab et al. (Abdelwahab 2014). Further, the addition of PDMS to luffa made it appropriate for absorbing crude oil and hazardous toxins. Luffa has a cheaper manufacturing cost than synthetic fibers and cotton, which results in lower pricing for the end product. It is feasible to salvage it from discarded items such as life preservers, upholstery, and bedding to recycle it as an oil sorbent, which would be beneficial to the environment. Because it is susceptible to biodegradation, it might, in the end, be thrown away to recover energy from biomass. As a consequence, the utilization of it does not lead to any secondary waste that is

ultimately released into the environment. The outcomes revealed that the process optimized for reusability of the scaffolds had notably facilitated their oil absorption capacity up to 10-12 times, and medium-sized P-L flakes showed significantly a great level of oil absorption capacity. Overall, this research provides a promising approach for designing and developing an optimal absorbent material for environmental remediation.

Table 4.9: Comparison of materials, fabrication methods, oils, and the absorption and adsorption capacities of various materials for oil-water separation.

Material used	Fabrication method	Scaffold dimension	Method/ formula/ units/ percentage	Types of oil	Advantages	Disadvantages	References
Silicon-modified polyester material	Chemical vapor deposition	5cm×5cm	separation efficiency (η) > 97% $\eta = \frac{m_1}{m_0} \times 100\%$ m_1= water mass before oil separation, m_0= water mass after separation	Diiodomethane, dichlorome, chloroform	Enhanced separation efficiency. High stability.	Requires prior water collection and may not be utilized directly at the designated site.	(Chowdhury, 2017; Ma et al., 2018; Mao et al., 2023; J. Zhang & Seeger, 2011)
Wax-modified natural sponge (ex. Luffa sponge)	Solution immersion/ Dip coating	size: 2cm-4cm diameter: 20µm	absorption capacity (K_{ac}) >10g/g $K_{ac} = \frac{m_{sa} - m_0}{m_0}$ m_{sa}= water mass prior to oil separation m_0= water mass after separation	Hexadecane, kerosene, chloroform, gasoline	Potential for sample recycling. usability over a wide pH range.	Require critical selection of the type of wax to avoid dissolution in oil/water	(F. Wang, Lei, et al., 2019; F. Wang, Xie, et al., 2019)

PDMS-coated PVDF nanofibers	**Poly[(3,3,3-trifluoropropyl) methylsiloxane] (PTFPMS)-modified membrane**	**Polydimethylsiloxane (PDMS)-modified metallic mesh**
Electrospinning	Dip coating	Dip coating
membrane area ≈ 770 $cm^{2,}$ thickness = 90 µm	Effective area ≈ 12cm^2	6 cm×6 cm diameter: 25µm
separation efficiency ≈ 99% $S = \left(1 - \frac{C_p}{C_f}\right) \times 100\%$ $C_f\ (ppm)$= water concentration before separation $C_p(ppm)$= water concentration after separation	separation efficiency (η) ≈ 98% $\eta = \frac{M}{M_0} \times 100\%$ M = mass before oil adsorption M_0= mass after adsorption	absorption capacity (k) ≈ 20 g/g Separation efficiency> 95% $k = \frac{W_a - W_b}{W_b}$ W_a= weight in the saturated state W_b = weight immediately after oil separation separation efficiency = $\frac{V_a}{V_b} \times 100\%$, V_a = liquid volume before oil separation V_b = liquid volume after oil separation
n-octane, n-hexane, toluene	Kerosene	Silicon oil, motor oil, diesel, kerosene
Superior surface hydrophobicity and lipophilicity.	High stability and reusability. Effective even in harsh conditions.	Relatively inexpensive and simple fabrication procedure. facilitates removal of oil spills.
Due to their incompatibility, it can be difficult to choose a solvent for the dissolution of PDMS and PVDF.	Loss of PTFPMS coatings may occur causing a reduction in the water contact angle	Less effective compared to carbon sponges, films, and aerogels.
(Cheng et al., 2021; J. Li et al. 2022)	(Hou et al., 2015, 2016)	Abdulhussein et al., 2019; Lipika & Singh, 2022)

Polystyrene-modified foams	**Inorganic nanoparticles-coated polyurethane foam**	**Polybenzoxazine-based cotton fabric**
Pickering emulsion polymerization	Dip coating	Dip coating
Not applicable	4cm×2cm×2cm	3cm×3cm
adsorption capacity (k) >7g/g $k = \frac{M_{sat} - M_0}{M_0}$ M_{sat}= weight of foam after oil adsorption M_0= mass of original dried foam	separation efficiency (e) ≈ 99% $e = \frac{V - V^0}{V} \times 100\%$ V= liquid volume prior to oil separation V^0= liquid volume lost during the separation	separation efficiency > 92% separation efficiency= $\frac{M_1}{M_0} \times 100\%$ M_1= mass of cotton fabric before adsorption M_0= mass after adsorption
Diesel, edible oil, toluene	Crude oil, diesel, gasoline, kerosene	Toluene, petroleum ether, cyclohexane, diesel
Superior reusability. Enhanced hydrophobicity and oleophilicity.	Excellent lipophilicity for a wide range of oils. Effective in continual oil removal.	Stable even in harsh conditions. excellent durability
Density and viscosity of oils affect oil adsorption.	Exhibits substantially lower adsorption rates for oils with high viscosity.	Has a relatively lower water contact angle in comparison to the silica-modified fabric.
(Udayakumar et al., 2021; N. Zhang et al., 2017)	(S. A. Khan et al., 2017; H.-D. Liu et al., 2018; Satria & Saleh, 2022)	(Bai et al., 2020; Y. Li et al., 2018; Shang et al., 2021)

Luffa cylindrica (LC) / PDMS	**Polydimethylsiloxane (PDMS) based melamine sponge**	**Cellulose-based fabrics**
Hand lay-up technique	Solution immersion	Polymer grafting
Diameter = 10 mm Thickness = 3 mm	Thickness = 2 cm	fabric area= 64 cm^2
Absorption capacity (%) $= \left(\frac{W_w - W_d}{W_d}\right) \times 100$ W_d= dry weight of the sample W_w= wet weight of the sample P-L mat = 16.09 ± 4.62% P-L flakes = 24.49 ±3.55% P-L powder = 15.52 ± 2.67% PDMS= 5.52 ± 1.44%	absorption capacity (k) ≈ 55 g/g $k = \frac{m_1 - m_0}{m_0}$ m_1= weight of the saturated sponge m_0= weight of the unsaturated PDMS-coated sponge	separation efficiency > 95% separation efficiency= $\frac{W_c}{W_p} \times 100\%$ W_c= weight of water dissipated by the fabric W_p= weight of water introduced into the fabric
Motor oil, organic solvents:Toluene, n- hexane, diethyl ether, cyclohexane	Chloroform, silicone oil, cyclohexane.	Hexadecane, chloroform, toluene, gasoline
Excellent oleophilic High stability even in harsh conditions. Multiple reusabilities.	Allows usage over a wide range of oils. Enhanced porosity and oleophilicity	Exhibited stability even in extreme condition Sample recycling is possible.
Requires improvement in absorption percentages.	Requires a vacuum pump system to facilitate continuous oil removal.	relatively lower water contact angles
current work	(Chen et al., 2016; Peng et al., 2018)	(Dan et al., 2020; Wei et al., 2020)

4.5 Conclusion

Various forms of luffa-PDMS composite scaffolds were fabricated using hand lay-up approach. Numerous characterizations were performed, including surface roughness, porosity, surface wettability, oil and PBS absorption, degradation, thermal stability, oil spillage and mechanical properties. The morphological analysis of SEM images showed the internal architecture of luffa, depicting microcapillaries and microporous structures. The P-L flakes scaffold had a high density of luffa microparticles resulting in the highest level of oil absorption. In contrast, the P-L powder appeared as an agglomerated material due to the majority of compromised capillaries. AFM images depicted that the P-L flakes scaffold had the highest surface roughness, a higher surface area-to-volume ratio, higher peak frequencies and more crests. The surface of P-L powder scaffolds exhibited fewer peaks with fewer peaks numbers due to its more tightly packed structure; reducing the microporous architecture. The existence of luffa within scaffolds exhibited exceptional oleophilic and PDMS displayed outstanding swelling in organic solvents. The P-L flakes have demonstrated a noticeably higher capacity for absorbing oil, PBS, and a few organic solvents, probably because of the high microcapillary properties of luffa flakes. The oxygen permeability of PDMS can enable continuous gaseous exchange between the water body and the atmosphere. In addition, the hydrophobic characteristics of PDMS enables buoyant forces to overcome the weight of the luffa-PDMS composite membrane and prevent it from sinking. Cell cytotoxicity testing demonstrates the cellular biocompatibility of the luffa-PDMS composite, indicating that it poses no threat to aquatic environments. Luffa fibers are found excellent for absorbing oil and adding PDMS render them suitable for absorbing crude oil toxic materials. The fabricated scaffolds can be reutilized 10-12 times proficiently. Moreover, luffa has lower production costs than synthetic fibers and cotton, resulting in lower end-product prices. This easy and green synthesis method can produce vast quantities of a multifunctional biomass-based adsorbent material for anti-fouling,

self-cleaning, and customized oil-water separation. Thus, the outcomes suggest that luffa-PDMS-based scaffolds might be a desired material for various environmental remediation applications.

4.6 References

Abdelwahab, Ola. 2014. "Assessment of Raw Luffa as a Natural Hollow Oleophilic Fibrous Sorbent for Oil Spill Cleanup." *Alexandria Engineering Journal* 53 (1): 213–18. https://doi.org/10.1016/j.aej.2013.11.001.

Abdulhussein, Ali T., Ganesh K. Kannarpady, and Alexandru S. Biris. 2019. "One-Step Synthesis of a Steel-Polymer Wool for Oil-Water Separation and Absorption." *Npj Clean Water* 2 (1): 10. https://doi.org/10.1038/s41545-019-0034-1.

Adebajo, M.O., R.L. Frost, J.T. Kloprogge, O. Carmody, and S. Kokot. 2003. "Porous Materials for Oil Spill Cleanup: A Review of Synthesis and Absorbing Properties." *Journal of Porous Materials* 10 (3): 159–70. https://doi.org/10.1023/A:1027484117065.

Akther, Fahima, Shazwani Binte Yakob, Nam-Trung Nguyen, and Hang T. Ta. 2020. "Surface Modification Techniques for Endothelial Cell Seeding in PDMS Microfluidic Devices." *Biosensors* 10 (11): 182. https://doi.org/10.3390/bios10110182.

Ali, Norizan, Mohanad El-Harbawi, Ayman Jabal, and Chun-Yang Yin. 2011. "Characteristics and Oil Sorption Effectiveness of Kapok Fibre, Sugarcane Bagasse and Rice Husks: Oil Removal Suitability Matrix." *Environmental Technology* 33 (January): 481–86. https://doi.org/10.1080/ 09593330.2011.579185.

Anastopoulos, Ioannis, and I. Pashalidis. 2020. "Environmental Applications of Luffa Cylindrica-Based Adsorbents." *Journal of Molecular Liquids*, August. https://doi.org/10.1016/j.molliq.2020.114127.

Bai, Weibin, Haimen Lin, Kunhui Chen, Jie Xu, Jipeng Chen, Xinmei Zhang, Renping Zeng, Jinhuo Lin, and Yanlian Xu. 2020. “Eco-Friendly Stable Cardanol-Based Benzoxazine Modified Superhydrophobic Cotton Fabrics for Oil–Water Separation.” *Separation and Purification Technology* 253 (December): 117545. https://doi.org/10.1016/j.seppur.2020.117545.

Bayraktaroglu, Seda, Soner Kizil, and Hayal Bulbul Sonmez. 2021. “A Highly Reusable Polydimethylsiloxane Sorbents for Oil/Organic Solvent Clean-up from Water.” *Journal of Environmental Chemical Engineering* 9 (5): 106002. https://doi.org/10.1016/j.jece.2021.106002.

Chen, Xuemei, Justin A. Weibel, and Suresh V. Garimella. 2016. “Continuous Oil–Water Separation Using Polydimethylsiloxane-Functionalized Melamine Sponge.” *Industrial & Engineering Chemistry Research* 55 (12): 3596–3602. https://doi.org/10.1021/acs.iecr.6b00234.

Cheng, Xi Quan, Yang Jiao, Zekun Sun, Xiaobin Yang, Zhongjun Cheng, Qing Bai, Yingjie Zhang, Kai Wang, and Lu Shao. 2021. “Constructing Scalable Superhydrophobic Membranes for Ultrafast Water–Oil Separation.” *ACS Nano* 15 (2): 3500–3508. https://doi.org/10.1021/acsnano.1c00158.

Choi, Sung-Jin, Tae-Hong Kwon, Hwon Im, Dong-Il Moon, David J. Baek, Myeong-Lok Seol, Juan P. Duarte, and Yang-Kyu Choi. 2011. “A Polydimethylsiloxane (PDMS) Sponge for the Selective Absorption of Oil from Water.” *ACS Applied Materials & Interfaces* 3 (12): 4552–56. https://doi.org/10.1021/am201352w.

Chowdhury, Subhendu Ray. 2017. “Advancement of Oil/Water Separating Materials: Merits and Demerits in Real-Time Applications.” *MOJ Polymer Science* 1 (1). https://doi.org/10.15406/mojps.2017.01.00003.

Cirer-Costa, Joan Carles. 2015. “Tourism and Its Hypersensitivity to Oil Spills.” *Marine Pollution Bulletin* 91 (1): 65–72. https://doi.org/10.1016/j.marpolbul.2014.12.027.

Dan, Yoav, Yanay Popowski, Marina Buzhor, Eti Menashe, Oren Rachmani, and Elizabeth Amir. 2020. “Covalent Surface Modification of Cellulose-Based Textiles for Oil–Water Separation Applications.” *Industrial & Engineering Chemistry Research* 59 (13): 5456–65. https://doi.org/10.1021/acs.iecr.9b05785.

Demir, H., U. Atikler, D. Balköse, and F. Tıhmınlıoğlu. 2006. “The Effect of Fiber Surface Treatments on the Tensile and Water Sorption Properties of Polypropylene–Luffa Fiber Composites.” *Composites Part A: Applied Science and Manufacturing* 37 (3): 447–56. https://doi.org/10.1016/j.compositesa. 2005.05.036.

Futalan, Cybelle Morales, Angelo Earvin S. Choi, Hannah Georgia O. Soriano, Melbourne Klein B. Cabacungan, and Jeremiah C. Millare. 2022. “Modification Strategies of Kapok Fiber Composites and Its Application in the Adsorption of Heavy Metal Ions and Dyes from Aqueous Solutions: A Systematic Review.” *International Journal of Environmental Research and Public Health* 19 (5): 2703. https://doi.org/10.3390/ijerph19052703.

Ge, Junyan, Yuxin Jia, Chuang Cheng, Ke Sun, Yuying Peng, Yingfang Tu, Yingying Qiang, et al. 2021. “Polydimethylsiloxane-Functionalized Polyacrylonitrile Nanofibrous Aerogels for Efficient Oil Absorption and Oil/Water Separation.” *Journal of Applied Polymer Science* 138 (45): 51339. https://doi.org/ 10.1002/app.51339.

Guan, Jianjun, Kazuro L. Fujimoto, Michael S. Sacks, and William R. Wagner. 2005. “Preparation and Characterization of Highly Porous, Biodegradable Polyurethane Scaffolds for Soft Tissue Applications.” *Biomaterials* 26 (18): 3961–71. https://doi.org/10.1016/j.biomaterials.2004.10.018.

Gundu, Shravanya, Ajay Kumar Sahi, Neelima Varshney, Johny Varghese, Niraj K Vishwakarma, and Sanjeev Kumar Mahto. 2022. “Fabrication and in Vitro Characterization of Luffa-Based Composite Scaffolds Incorporated with Gelatin, Hydroxyapatite and Psyllium Husk for Bone Tissue Engineering.” *Journal of Biomaterials Science. Polymer Edition*, July, 1–29. https://doi.org/10.1080/09205063.2022.2101415.

Guo, Jiahong, Jikui Wang, Wenqi Wang, Zhiwei Bai, Zhibing Zhang, Yajuan Zhang, and Shiping Zhang. 2019. “The Fabrication of 3D Porous PDMS Sponge for Oil and Organic Solvent Absorption.” *Environmental Progress & Sustainable Energy* 38 (s1): S86–92. https://doi.org/10.1002/ep.12924.

Hou, Yi, Chun-ting Duan, Ning Zhao, Huan Zhang, Yi-ping Zhao, Li Chen, Hong-jun Dai, and Jian Xu. 2016. “A Versatile Coating Approach to Fabricate Superwetting Membranes for Separation of Water-in-Oil Emulsions.” *Chinese Journal of Polymer Science* 34 (10): 1234–39. https://doi.org/10.1007/s10118-016-1828-y.

Hou, Yi, Zhen Wang, Jing Guo, Heng Shen, Huan Zhang, Ning Zhao, Yiping Zhao, et al. 2015. “Facile Fabrication of Robust Superhydrophobic Porous Materials and Their Application in Oil/Water Separation.” *Journal of Materials Chemistry A* 3 (46): 23252–60. https://doi.org/10.1039/C5TA05612H.

Khan, Mohd Jahir, Ramesh Singh, Khashti Ballabh Joshi, and Vandana Vinayak. 2019. “TiO2 Doped Polydimethylsiloxane (PDMS) and Luffa Cylindrica Based Photocatalytic Nanosponge to Absorb and Desorb Oil in Diatom Solar Panels.” *RSC Advances* 9 (39): 22410.

Khan, Sharjeel Ahmed, Usama Zulfiqar, Syed Zajif Hussain, Usama Zaheer, Irshad Hussain, Syed Wilayat Husain, and Tayyab Subhani. 2017. “Fabrication of Superhydrophobic Filter Paper and Foam for Oil–Water Separation Based on Silica Nanoparticles from

Sodium Silicate." *Journal of Sol-Gel Science and Technology* 81 (3): 912–20. https://doi.org/10.1007/s10971-016-4250-6.

Kim, Daehan, Sung-Hwan Kim, and Joong Yull Park. 2019. "Floating-on-Water Fabrication Method for Thin Polydimethylsiloxane Membranes." *Polymers* 11 (8): 1264. https://doi.org/10.3390/polym11081264.

Laitinen, Ossi, Terhi Suopajärvi, Monika Österberg, and Henrikki Liimatainen. 2017. "Hydrophobic, Superabsorbing Aerogels from Choline Chloride-Based Deep Eutectic Solvent Pretreated and Silylated Cellulose Nanofibrils for Selective Oil Removal." *ACS Applied Materials & Interfaces* 9 (29): 25029–37. https://doi.org/10.1021/acsami.7b06304.

Lamberti, A., S. L. Marasso, and M. Cocuzza. 2014. "PDMS Membranes with Tunable Gas Permeability for Microfluidic Applications." *RSC Advances* 4 (106): 61415–19. https://doi.org/10.1039/C4RA12934B.

Li, Jie, Yushan Li, Yiyi Lu, Wentian Shi, and Huafeng Tian. 2022. "PDMS/PVDF Electrospinning Membranes for Water-in-Oil Emulsion Separation and UV Protection." *Biomimetics* 7 (4): 217. https://doi.org/10.3390/biomimetics7040217.

Li, Yun, Qiao Yu, Xianze Yin, Jing Xu, Yajun Cai, Lu Han, Hao Huang, et al. 2018. "Fabrication of Superhydrophobic and Superoleophilic Polybenzoxazine-Based Cotton Fabric for Oil–Water Separation." *Cellulose* 25 (11): 6691–6704. https://doi.org/10.1007/s10570-018-2024-8.

Lipika, and Arun K. Singh. 2022. "Polydimethylsiloxane Based Sustainable Hydrophobic/Oleophilic Coatings for Oil/Water Separation: A Review." *Cleaner Materials* 6 (December): 100136. https://doi.org/10.1016/j.clema.2022.100136.

Liu, Hai-Dong, Bin Gu, Wei-Feng Yuan, and Qi He. 2018. “Fabrication of a Superhydrophobic Polyurethane Foam and Its Application for Continuous Oil Removal.” *Materials Research Express* 5 (2): 025005. https://doi.org/10.1088/ 2053-1591/aaa995.

Liu, Liao, Jiannan Chen, Wuhuan Zhang, Meikun Fan, Zhengjun Gong, and Jianqiang Zhang. 2020. “Graphene Oxide/Polydimethylsiloxane Composite Sponge for Removing Pb(II) from Water.” *RSC Advances* 10 (38): 22492–99. https://doi.org/10.1039/D0RA03057K.

Lv, Na, Xiaoli Wang, Shitao Peng, Lei Luo, and Ran Zhou. n.d. “Superhydrophobic/Superoleophilic Cotton-Oil Absorbent: Preparation and Its Application in Oil/Water Separation.” *RSC Advances* 8 (53): 30257–64. https://doi.org/10.1039/c8ra05420g.

Ma, Qi, Bin Wang, Jilei Xu, Junwei Lv, Hui Li, Yuntao Li, and Chunxia Zhao. 2018. “Preparation of Super-Hydrophobic Polyester Fabric by Growing Polysiloxane Microtube and Its Application.” *Silicon* 10 (5): 2009–14. https://doi.org/10.1007/ s12633-017-9714-y.

Mao, Taoyan, Runhui Xiao, Peng Liu, Jiale Chen, Junqiang Luo, Su Luo, Fengwei Xie, and Cheng Zheng. 2023. “Facile Fabrication of Durable Superhydrophobic Fabrics by Silicon Polyurethane Membrane for Oil/Water Separation.” *Chinese Journal of Chemical Engineering* 55 (March): 73–83. https://doi.org/10.1016/ j.cjche.2022.05.003.

Markov, Dmitry A., Elizabeth M. Lillie, Shawn P. Garbett, and Lisa J. McCawley. 2014. “Variation in Diffusion of Gases through PDMS Due to Plasma Surface Treatment and Storage Conditions.” *Biomedical Microdevices* 16 (1): 91–96. https://doi.org/10.1007/s10544-013-9808-2.

Menya, E., P. W. Olupot, H. Storz, M. Lubwama, and Y. Kiros. 2018. “Production and Performance of Activated Carbon from Rice Husks for Removal of Natural Organic Matter from Water: A Review.” *Chemical Engineering Research and Design* 129 (January): 271–96. https://doi.org/10.1016/j.cherd.2017.11.008.

Miranda, Inês, Andrews Souza, Paulo Sousa, João Ribeiro, Elisabete Castanheira, Rui Lima, and Graca Minas. 2021. “Properties and Applications of PDMS for Biomedical Engineering: A Review.” *Journal of Functional Biomaterials* 13 (December): 2. https://doi.org/10.3390/jfb13010002.

Ong, Chong Cheen, Satisvar Sundera Murthe, Norani Muti Mohamed, Veeradasan Perumal, and Mohamed Shuaib Mohamed Saheed. 2018. “Nanoscaled Surface Modification of Poly(Dimethylsiloxane) Using Carbon Nanotubes for Enhanced Oil and Organic Solvent Absorption.” *ACS Omega* 3 (11): 15907–15. https://doi.org/10.1021/acsomega.8b01566.

Park, Eunhee, and Jaehyun Hur. 2021. “Three-Dimensionally Interconnected Porous PDMS Decorated with Poly(Dopamine) and Prussian Blue for Floatable, Flexible, and Recyclable Photo-Fenton Catalyst Activated by Solar Light.” *Applied Surface Science* 545 (April): 148990. https://doi.org/10.1016/j.apsusc.2021.148990.

Peng, Jinwen, Junjie Deng, Yiteng Quan, Chuanbai Yu, Hai Wang, Yongyang Gong, Yuanli Liu, and Weixing Deng. 2018. “Superhydrophobic Melamine Sponge Coated with Striped Polydimethylsiloxane by Thiol–Ene Click Reaction for Efficient Oil/Water Separation.” *ACS Omega* 3 (5): 5222–28. https://doi.org/10.1021/acsomega.8b00373.

Satria, Mauliady, and Tawfik A. Saleh. 2022. “Effect of Loading Various Nanoparticles on Superhydrophobic/Superoleophilic Stearic Acid-Modified Polyurethane Foams for Oil-Water Separation.” *Journal of Environmental Chemical Engineering* 10 (6): 108577. https://doi.org/10.1016/j.jece.2022.108577.

Sayed, S. A., and A. M. Zayed. 2006. “Investigation of the Effectiveness of Some Adsorbent Materials in Oil Spill Clean-Ups.” *Desalination* 194 (1): 90–100. https://doi.org/10.1016/j.desal.2005.10.027.

Seki, Yoldas, Kutlay Sever, Seckin Erden, Mehmet Sarikanat, Gökdeniz Neser, and Cicek Ozes. 2012. “Characterization of Luffa Cylindrica Fibers and the Effect of Water Aging on the Mechanical Properties of Its Composite with Polyester.” *Journal of Applied Polymer Science* 123 (4): 2330–37. https://doi.org/10.1002/app.34744.

Senanurakwarkul, C., P. Khongsricharoen, D. Pejprom, S. Tantayanon, and S. Khaodhiar. 2013. “Effects of the Composition and the Preparation Methods on Oil Sorption Capacity of Recycled Rayon Waste-Kapok Mixtures (RRWK) Sorbent.” *International Journal of Environmental Science and Development* 4 (3): 246–50.

Shang, Qianqian, Jianwen Cheng, Chengguo Liu, Lihong Hu, Caiying Bo, Yun Hu, Xiaohui Yang, Xiaoli Ren, Yonghong Zhou, and Wen Lei. 2021. “Fabrication of Sustainable and Durable Bio-Polybenzoxazine Based Superhydrophobic Cotton Fabric for Efficient Oil/Water Separation.” *Progress in Organic Coatings* 158 (September): 106343. https://doi.org/10.1016/j.porgcoat.2021.106343.

Singh, Harpreet, Neha Bhardwaj, Shailendra Kumar Arya, and Madhu Khatri. 2020. “Environmental Impacts of Oil Spills and Their Remediation by Magnetic Nanomaterials.” *Environmental Nanotechnology, Monitoring & Management* 14 (December): 100305. https://doi.org/10.1016/j.enmm.2020.100305.

Singh, Vinitkumar, Sudheer Jinka, Kater Hake, Siva Parameswaran, Ronald J. Kendall, and Seshadri Ramkumar. 2014. “Novel Natural Sorbent for Oil Spill Cleanup.” *Industrial & Engineering Chemistry Research* 53 (30): 11954–61. https://doi.org/10.1021/ie5019436.

Solomon, Gina M., and Sarah Janssen. 2010. “Health Effects of the Gulf Oil Spill.” *JAMA* 304 (10): 1118–19. https://doi.org/10.1001/jama.2010.1254.

Udayakumar, Kavitha Vellopollath, Prakash M. Gore, and Balasubramanian Kandasubramanian. 2021. “Foamed Materials for Oil-Water Separation.” *Chemical Engineering Journal Advances* 5 (March): 100076. https://doi.org/10.1016/ j.ceja.2020.100076.

Vagos, Márcia R., Marisa Gomes, Joana M. R. Moreira, Olívia S. G. P. Soares, Manuel F. R. Pereira, and Filipe J. Mergulhão. 2020. “Carbon Nanotube/Poly (Dimethylsiloxane) Composite Materials to Reduce Bacterial Adhesion.” *Antibiotics* 9 (8): 434. https://doi.org/10.3390/antibiotics9080434.

Wang, Fajun, Sheng Lei, Junfei Ou, Changquan Li, and Wen Li. 2019. “Novel All-Natural Material for Oil/Water Separation.” *Industrial & Engineering Chemistry Research* 58 (5): 1924–31. https://doi.org/10.1021/acs.iecr.8b05535.

Wang, Fajun, Ting Xie, Wei Zhong, Junfei Ou, Mingshan Xue, and Wen Li. 2019. “A Renewable and Biodegradable All-Biomass Material for the Separation of Oil from Water Surface.” *Surface and Coatings Technology* 372 (August): 84–92. https://doi.org/10.1016/j.surfcoat.2019.05.002.

Wang, Zhe, Hongyang Ma, Benjamin Chu, and Benjamin S. Hsiao. 2017. “Super-Hydrophobic Modification of Porous Natural Polymer ‘Luffa Sponge’ for Oil Absorption.” *Polymer* 126 (September): 470–76. https://doi.org/10.1016/ j.polymer.2017.05.068.

Wei, David W., Haiying Wei, Alec C. Gauthier, Junlong Song, Yongcan Jin, and Huining Xiao. 2020. “Superhydrophobic Modification of Cellulose and Cotton Textiles: Methodologies and Applications.” *Journal of Bioresources and Bioproducts* 5 (1): 1–15. https://doi.org/10.1016/j.jobab.2020.03.001.

Wolok, Eduart, Jamal Barafi, Navneet Joshi, Rossella Girimonte, and Sudip Chakraborty. 2020. “Study of Bio-Materials for Removal of the Oil Spill.” *Arabian Journal of Geosciences* 13 (23): 1244. https://doi.org/10.1007/s12517-020-06244-3.

Xu, Yanfang, Cao Liyao, Hua Shen, and Guangbiao Xu. 2021. “Temperature Effect on Oil Sorption and Wettability of Kapok Fiber.” *Journal of Natural Fibers* 19 (January): 1–12. https://doi.org/10.1080/15440478.2020.1820931.

Yu, Cunlong, Cunming Yu, Liying Cui, Zhiyang Song, Xinyu Zhao, Ying Ma, and Lei Jiang. 2017. “Facile Preparation of the Porous PDMS Oil-Absorbent for Oil/Water Separation.” *Advanced Materials Interfaces* 4 (3): 1600862. https://doi.org/ 10.1002/ admi.201600862.

Yu, Mingguang, Binbin Lin, Shangxian Chen, Qianjun Deng, Guang Liu, and Qing Wang. 2018. “Biomimetic Fabrication of Superhydrophobic Loofah Sponge: Robust for Highly Efficient Oil–Water Separation in Harsh Environments.” *RSC Advances* 8 (January): 24297–304. https://doi.org/10.1039/C8RA04336A.

Zhai, Guanzhong, Lixue Qi, Wang He, Jiajun Dai, Yan Xu, Yanmei Zheng, Jiale Huang, and Daohua Sun. 2021. “Durable Super-Hydrophobic PDMS@SiO2@WS2 Sponge for Efficient Oil/Water Separation in Complex Marine Environment.” *Environmental Pollution* 269 (January): 116118. https://doi.org/10.1016/j.envpol. 2020.116118.

Zhang, Junping, and Stefan Seeger. 2011. “Polyester Materials with Superwetting Silicone Nanofilaments for Oil/Water Separation and Selective Oil Absorption.” *Advanced Functional Materials* 21 (24): 4699–4704. https://doi.org/10.1002/ adfm. 201101090.

Zhang, Ning, Suting Zhong, Teng Chen, Yu Zhou, and Wei Jiang. 2017. “Emulsion-Derived Hierarchically Porous Polystyrene Solid Foam for Oil Removal from Aqueous Environment.” *RSC Advances* 7 (37): 22946–53. https://doi.org/10.1039/ C7RA02953E.

Zhang, Wen, Juanjuan Wang, Xue Han, Lele Li, Enping Liu, and Conghua Lu. 2021. “Carbon Nanotubes and Polydopamine Modified Poly(Dimethylsiloxane) Sponges for Efficient Oil-Water Separation.” *Materials (Basel, Switzerland)* 14 (9): 2431. https://doi.org/10.3390/ma14092431.

Zheng, Xudong, Biao Ji, Rong Jiang, Yawen Cui, Tongtong Xu, Man Zhou, and Zhongyu Li. 2022. “Polydimethylsiloxane/Carbonized Bacterial Cellulose Sponge for Oil/Water Separation.” *Process Safety and Environmental Protection* 165 (September): 173–80. https://doi.org/10.1016/j.psep.2022.07.014.